KUOPION YLIOPISTON JULKAISUJA G. – A .I. VIRTANEN-INSTITUUTTI 6
KUOPIO UNIVERSITY PUBLICATIONS G. – A. I. VIRTANEN INSTITUTE FOR MOLECULAR SCIENCES 6

JOHANNA SILVENNOINEN

A Study of NMR Relaxation in Blood - Mechanistic Considerations and Implications for Quantitative Functional MRI

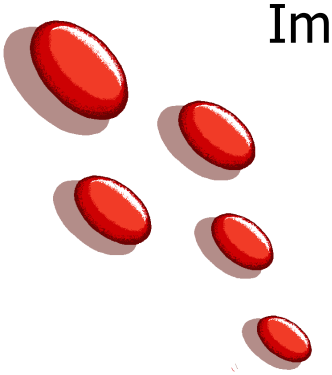

Johanna Silvennoinen

A Study of NMR Relaxation in Blood - Mechanistic Considerations and Implications for Quantitative Functional MRI

Doctoral Dissertation

To be presented by permission of the Faculty of Natural and Environmental Sciences of the University of Kuopio for public examination in Teknia Auditorium, University of Kuopio, on Saturday 7th December, 2002, at 12 noon

Department of Biomedical NMR and National Bio-NMR Facility
A.I.Virtanen Institute for Molecular Sciences
University of Kuopio

Kuopio 2002

Distributor: Kuopio University Library
P.O.Box 1627
70211 KUOPIO, FINLAND
Tel. +358 17 163 430
Fax +358 17 163 410

Series editors: Professor Karl Åkerman
Department of Neurobiology
A.I.Virtanen Institute for Molecular Sciences
University of Kuopio, Finland

Research Director Jarmo Wahlfors
Department of Biotechnology and Molecular Medicine
A.I.Virtanen Institute for Molecular Sciences
University of Kuopio, Finland

Author's address: Department of Biomedical NMR and National Bio-NMR Facility
A. I. Virtanen Institute for Molecular Sciences
University of Kuopio, Finland
P.O.Box 1627
70211 KUOPIO, FINLAND
Tel. +358 17 162 012
Fax +358 17 163 030

Supervisors: Professor Risto Kauppinen, M.D., Ph.D.
Department of Biomedical NMR
A.I.Virtanen Institute for Molecular Sciences
University of Kuopio, Finland

Professor Peter van Zijl, Ph.D.
Department of Radiology, Division of MR Research
Johns Hopkins Medical School
Baltimore, MD, USA

Reviewers: Professor Robert G. Bryant, Ph.D.
Department of Chemistry
University of Virginia
Charlottesville, VA, USA

Professor Chrit T. W. Moonen, Ph.D.
Résonance Magnétique des systèms Biologiques
Université Victor Segalen
Bordeaux, France

Opponent: Professor Pierre Gillis, Ph.D.
Service de Physique Expérimentale et Biologique
Université de Mons-Hainaut
Mons, Belgium

ISBN 915-781-956-X
ISSN 1458-7335
Kuopio University Printing Office
Kuopio 2002
Finland

Silvennoinen, Johanna. A Study of NMR Relaxation in Blood - Mechanistic Considerations and Implications for Quantitative Functional MRI. Kuopio University Publications G. – A.I.Virtanen Institute for Molecular Sciences 6. 2002. 61 p.
ISBN 915-781-956-X
ISSN 1458-7335

Abstract

Nuclear magnetic resonance (NMR) imaging (MRI) and spectroscopy (MRS) are invaluable tools in medical imaging, providing information on both the structure and the function of living systems in a noninvasive manner. The NMR signal and image contrast are product of several physical and physiological factors, the most important being NMR relaxation of the tissue. In the present study, blood was chosen as a model tissue, since it accounts for 7-8 % of body weight and approximately 4 % of gray matter. This study focused on the quantification of dynamic relaxation properties (relaxation times T_1, $T_{1\rho}$, T_2 and T_2*) of isolated blood as well as on the consequences of these properties on quantitative functional MRI (fMRI) applications.

In transverse NMR relaxation (CPMG-T_2, single-echo (Hahn) T_2 and T_2*), the expected blood oxygen level dependent (BOLD) behavior was observed and quantified at several hematocrits at 1.5 and 4.7 T. The blood CPMG results were utilized in the determination of oxygen extraction ratio *in vivo* in humans at 1.5 T. Moving from single spin echoes to gradient echoes (T_2*) was shown to add an oxygenation-independent term to the spin echo relaxation rate. The single and gradient echo data were used to simulate intravascular BOLD signal changes in fMRI experiments with neuronal activation both at 1.5 T and at 4.7 T.

The longitudinal relaxation in blood at 4.7 T was found to depend on hematocrit. Interestingly, some dependence on blood oxygenation also in both T_1 and $T_{1\rho}$ was observed, possibly arising from intramolecular relaxation in hemoglobin. The consequences of physiological variation in the blood parameters, and thus in T_1, in the determination of cerebral blood flow *in vivo* were evaluated and found to induce significant bias under conceivable conditions.

The study provides a thorough quantitative description of relaxation processes in blood and addresses their significance in different fMRI applications. In addition, a set of reference values are given for blood, at body temperature and over a wide range of oxygen saturation levels as well as hematocrits, for fMRI models of hemodynamics *in vivo*.

National Library of Medicine Classification: WN 185, WH 450, QY 400, QY 4098 WG 106, WL 302
Medical Subject Headings: diagnostic imaging; magnetic resonance imaging; magnetic resonance spectroscopy; blood; erythrocytes; hematocrit; hemoglobins; hemodynamics; brain; cerebrovascular circulation

Acknowledgements

The present study was carried out in the Department of Biomedical NMR, A. I. Virtanen Institute, University of Kuopio and in Department of Radiology, Johns Hopkins Medical School in 1998-2002.

This work would not exist without my principal supervisor, Professor Risto Kauppinen, MD PhD. He has taught me a lot; not only about science and research work but also about the attitude, spirit and enthusiasm that make the difference in this profession. For this I wish to express my deepest gratitude. The same words I could say about my other supervisor, Professor Peter van Zijl, PhD. He gave me the opportunity to work as member of his group in the F. M. Kirby Center and has been the power generator behind half of the papers in this study.

I thank the reviewers of this thesis, Professors Robert Bryant, PhD and Chrit Moonen, PhD, for their comments, ideas and constructive criticism. I also wish to acknowledge Dr. Ewen Macdonald, PhD, for his help with the language.

The two people who have made the experiments possible are Professor Xavier Golay, PhD and Dr. Mikko Kettunen, PhD. I am grateful for their willingness to share their time and knowledge and for their ideas and comments during the project. I also wish to thank the other co-authors, Professors Jim Pekar, PhD, and Jinyuan Zhou, PhD, for their contribution, and especially Chekesha Clingman, MSc, for sharing the joys of late-night blood experiments and cleaning out the mess from ripped tubings.

I am grateful to Dr. Olli Gröhn, PhD, and Dr. Juhana Hakumäki, MD, PhD for their help and comments in different stages of this work and to Dr. Jukka Häyrinen, PhD, for his expertise in biochemistry and helping me out with practical work in the lab. I wish to thank the rest of the people in the NMR group in Kuopio and in the Kirby Center in Baltimore. It has been a pleasure to work and have fun with you. A special, warm hug goes to our MR-mom, Terri Brawner, BS, RT.

Several foundations and organizations have given financial support to my work. I wish to thank the Aarne and Aili Turunen Foundation, Academy of Finland, the Finnish Cultural Foundation of Northern Savo, Finnish Graduate School of Neuroscience, Helena Vuorenmies Foundation, Instrumentarium Science Foundation, International Society for Magnetic Resonance in Medicine, Kuopio University Foundation, Magnus Ehrnrooth Foundation, Maud Kuistila Foundation and Sigrid Juselius Foundation. I also thank the Finnish Red Cross and Atria Ltd. for generously donating human and bovine blood samples used in this work.

I believe the foundation for my desire to learn to how things work has been built in my childhood. I am deeply grateful to my parents for lovingly supporting me and encouraging me to ask questions, read and investigate.

Finally, I would like to find words for express my love and gratitude to my personal PC-helpdesk, kayaking partner, electrician-plumber-carpenter and very best friend – my husband Jarkko. He has been the steady base for me during these years of traveling, in Finland and across the Atlantic, always encouraging me to go for my goals and willing to adapt his own plans. I owe him so much and I hope I can show him similar love and support in return.

Abbreviations

ASL	arterial spin labeling
B_0 field	main magnetic field
B_1,field	radio-frequency field
BOLD	blood oxygen level dependent
BSA	bovine serum albumin
CBF	cerebral blood flow
CBV	cerebral blood volume
$CMRO_2$	cerebral metabolic rate of oxygen
CPMG	Carr-Purcell-Meiboom-Gill multiecho
D	diffusion coefficient
D_{av}	1/3 of the trace of the diffusion tensor
GRE	gradient echo
γ	gyromagnetic ratio, 42.58 MHz / T for hydrogen
h	Planck's constant, 6.628×10^{-34} Js
Hb	hemoglobin
HbA	normal hemoglobin
HbS	sickle cell hemoglobin
Hct	hematocrit
metHb	methemoglobin
I	spin quantum number of a nucleus
IR	inversion recovery
k	Boltzmann constant, 1.381×10^{-23} J/Kelvin
M	net magnetization vector / signal intensity
M_0	steady-state magnetization
MRI	magnetic resonance imaging
MRS	magnetic resonance spectroscopy
MT	magnetization transfer
NMR	nuclear magnetic resonance
NMRD	nuclear magnetic resonance dispersion
OER	oxygen extraction ratio
$\Delta\omega$	magnetic susceptibility difference
ω_0	angular frequency of main magnetic field B_0
ω_1	angular frequency of RF field B_1
R_1	longitudinal relaxation rate ($1/T_1$)
$R_{1\rho}$	longitudinal relaxation rate ($1/T_{1\rho}$) in the rotating frame
R_2	intrinsic transverse relaxation rate ($1/T_2$)
R_2*	effective transverse relaxation rate ($1/T_2$*)
RF	radio-frequency
S	angular momentum (quantum number) of an atom
SAR	specific absorption rate

SE	spin-echo
SLT	spin-lock time
T_1	longitudinal relaxation time
$T_{1\rho}$	longitudinal relaxation time in the rotating frame
T_2	intrinsic transverse relaxation time
T_2^*	effective transverse relaxation time
τ_c	correlation time
τ_{ery}	residence time (of water) in erythrocytes
τ_{exch}	exchange time
τ_{CPMG}	delay for a echo refocusing in a CPMG experiment
TE	time to echo, “echo time”
TI	time from inversion, "inversion time"
TR	time to repeat, “repetition time”
x_{deoxy}	fraction of deoxygenated hemoglobin
Y	oxygenation

List of original publications

I **Effects of Hematocrit and Oxygen Saturation on the Blood Spin-Lattice Relaxation**
M. Johanna Silvennoinen, Mikko I. Kettunen, Risto A. Kauppinen
Magnetic Resonance in Medicine: *in press*

II **Blood NMR Relaxation in the Rotating Frame: Mechanistic Implications**
M. Johanna Silvennoinen, Mikko I. Kettunen, Chekesha S. Clingman, Risto A. Kauppinen
Archives of Biochemistry and Biophysics 405: 78-86, 2002

III **Measurement of Tissue Oxygen Extraction Ratios from Venous Blood: Increased Precision and Validation of Principle**
Xavier Golay, M. Johanna Silvennoinen, Jinyuan Zhou, Chekesha S. Clingman, Risto A. Kauppinen, James J. Pekar, Peter C. M. van Zijl
Magnetic Resonance in Medicine 46: 282-291, 2001

IV **Comparison of the Dependence of Blood R_2 and R_2* on Oxygen Saturation at 1.5 and 4.7 Tesla**
M. Johanna Silvennoinen, Chekesha S. Clingman, Xavier Golay, Risto A. Kauppinen, Peter C. M. van Zijl
Magnetic Resonance in Medicine: *in press*

Table of contents

And because this experimental science is a study entirely unknown by the common people, I cannot convince them of its utility, unless its virtue and characteristics are shown. This alone enables us to find out surely what can be done through nature, what through the application of art, what through fraud, what is the purport and what is mere dream in chance, conjuration, invocations, imprecations, magical sacrifices and what there is in them; so that all falsity may be lifted and the truths we alone of the art retained.

Roger Bacon: On Experimental Science, 1268

1 INTRODUCTION

The applications of nuclear magnetic resonance (NMR) methods - magnetic resonance imaging (MRI) and magnetic resonance spectroscopy (MRS) - provide a versatile tool for exploring structure and function of materials. As the methods are fully noninvasive and produce no dose of ionizing radiation, they are excellent for studies of living objects, ranging from cells to man. In addition to anatomical and structural information, an MRI experiment can be designed to provide quantitative information on dynamic events, such as diffusion of water (Moseley et al., 1990), blood flow (Williams et al., 1992) and volume (van Zijl et al., 1998) and oxygen consumption (Ogawa et al., 1993). By labeling specific molecules with MRI contrast agents, distribution of these compounds (upon drug release or gene expression, for instance) can be imaged (Weissleder et al., 2000). In spectroscopy, different chemical compounds can be detected and their properties studied.

In most living tissue, vasculature is an inherent and dynamic part of the organ. In order to model the NMR signal in such a complicated system, knowledge on the vascular dynamics and the NMR characteristics of blood are important. From the NMR point of view, blood is a complex material. In addition to its inhomogeneous structure, its several components are also dynamic. The red blood cell density, i. e. hematocrit (Hct), varies between individuals as well as within the same subject, and oxygen balance is known to affect the magnetic properties of hemoglobin molecules, resulting in blood oxygenation dependent (BOLD) signal behavior. All of these parameters influence the NMR characteristics, especially spin relaxation, of blood. Transverse relaxation in blood has been studied from several directions. Mechanistic studies on membrane permeability (Andrasko, 1976; Benga and Borza, 1995) and relaxation mechanisms (Brooks et al., 1989; Gillis and Koenig, 1987) as well as calibration measurements (Li et al., 1998; Wright et al., 1991) have been carried out. With respect to gradient echo data, the reports (Barth and Moser, 1997; Chien et al., 1994; Li et al., 1998; Spees et al., 2001) are more sparse and the results vary greatly. Reports on longitudinal relaxation deal mainly with magnetic field dispersion while the effects of oxygenation and hematocrit have been discussed less extensively

(Bryant et al., 1990). A review encompassing these aspects at a general level was provided by Brooks and Di Chiro in 1987 (Brooks and Di Chiro, 1987).

In this work, both transverse and longitudinal relaxation rate constants in blood have been quantified systematically, in as natural blood as possible *in vitro* at body temperature. The analysis has focused on the effect of physiologically relevant dynamic parameters (oxygenation, hematocrit) and, in a qualitative manner, field strength. The objectives are as follows: Firstly, the study complements the tools needed in quantitative modeling of physiology *in vivo* using NMR. This was tested by applying the results in the determination of the oxygen extraction ratio (OER) *in vivo*. Secondly, the data are interpreted in the light of different relaxation mechanisms. In addition to being of academic interest, understanding the mechanistic aspects is essential in developing new methods for *in vivo* applications.

2 REVIEW OF THE LITERATURE

2.1 Blood and vasculature

2.1.1 Composition and function of blood

Blood accounts for approximately 8 % of the body weight of most mammals, including humans. Blood carries and delivers oxygen, water, nutrients and hormones to the tissues and transports their waste products. It is also a crucial component of thermoregulation, as it absorbs and redistributes excess heat in the body. The acid – base balance in blood is a critical factor in body functions, e.g. in gas exchange in respiratory system. The main components of blood are plasma and red blood cells which contain hemoglobin (Hb) at a 5 mM concentration. White blood cells, leukocytes, and platelets occupy less than one percent of the total blood volume (Guyton, 1986).

Plasma contains mostly water; the 6-7 % protein fraction mainly consists of albumin (~70 kD), fibrinogen (~340 kD) and globulins (~160 kD). Albumin, the most abundant plasma protein, is important in transporting substances as well as in maintaining the osmotic pressure in capillaries. It is also involved in regulating blood pressure and blood flow. Globulins participate in transport processes as well as in blood clotting, together with fibrinogen. Immunoglobulins are important components of defense mechanisms. Plasma also contains small amounts of nutrients, gases, hormones, electrolytes and waste products (Guyton, 1986).

2.1.1.1 Erythrocytes

Red blood cells, erythrocytes, are specialized cells for delivering oxygen from the lungs to the rest of the body. The volume fraction occupied by erythrocytes, the hematocrit, varies in healthy subjects between 0.38 and 0.50. In the normal cerebral microvasculature, hematocrit drops to 85 % of the macrovascular hematocrit but in pathological tissue, such as in tumors, the microvascular hematocrit varies greatly. The shape of an erythrocyte is a biconcave disk; the diameter is 6-8 μm with thickness at its center less than 1 μm. The cell size and shape varies little between most mammalian species. The shape maximizes the surface area for O_2 diffusion and minimizes the diffusion distance in the cell. It also permits extensive deformations, a characteristic needed in passage through micrometer-scale capillaries, as well as large changes in the cell volume. Under hypotonic conditions, an erythrocyte can almost double its volume, achieving a spherical form, but if excessive changes in surface area are required, the cell will rupture, resulting in hemolysis (Fig. 1). Mammalian erythrocytes contain neither a nucleus nor mitochondria and their small energy demand is fulfilled by anaerobic metabolism. The cells remain functional only for approximately four months and thereafter the cells are removed by the spleen (Hoffman et al., 2000).

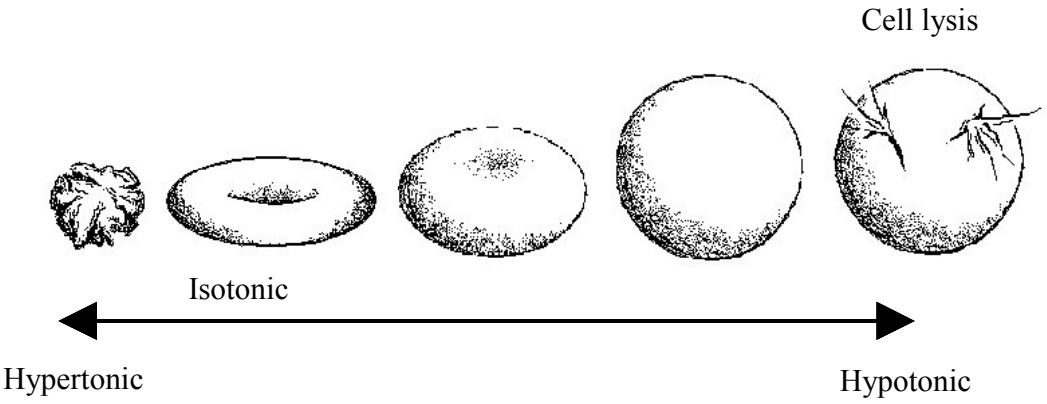

Figure 1: Erythrocyte shape in solutions of different osmolarities

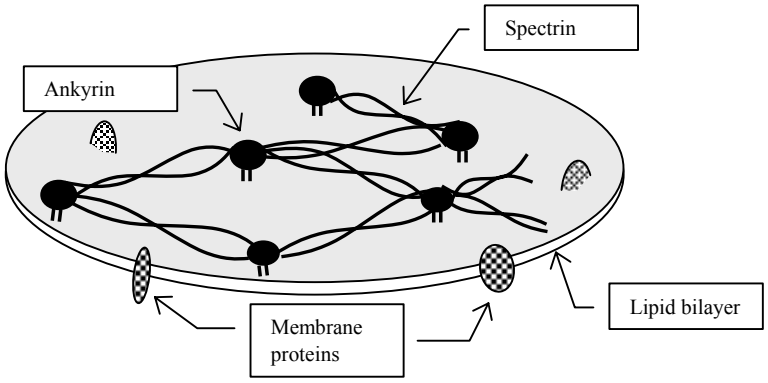

Figure 2: Plasma membrane and cytoskeleton

The erythrocyte membrane is probably the best-studied biological membrane, as the cells are easily available and the membrane can be readily isolated. The membrane is a standard biological lipid bilayer (Hoffman et al., 2000) with the main membrane proteins being glycophorin A and band-3 protein. The flexible cytoskeleton consists of a filamentous spectrin meshwork, which is attached to the membrane by a bond between ankyrin and band-3 protein (Fig. 2). Water moves easily through the membrane. The main water channel, aquaporin-1 is responsible for most of the water exchange (>64 % of diffusional permeability and >85% of the osmotic permeability (Mathai et al., 1996)). The length of this channel is about 50 Å and the average transit rate is $3*10^9$ molecules/s (Heymann et al., 1998). The average residence time of water in erythrocytes (τ_{ery}) is 12 ms at body temperature and close to 20 ms at room temperature in human erythrocytes. This exchange rate can be slowed down by using water channel blocking agents such as p-chloromercuribenzenesulfonate (pCMBS) and sulfhydryl (SH) reagents (Benga, 1989). The average exchange rate across the cell membrane in terms of residence times in erythrocytes and plasma can be expressed:

$$\tau_{exch}^{-1} = \tau_{ery}^{-1} + \tau_{plasma}^{-1} \Rightarrow \tau_{exch} = (1 - Hct)\tau_{ery} \qquad \textbf{Equation 1}$$

In plasma, the motion of water is free and the diffusion coefficient is close to that in pure water (Gillis et al., 1995). Intracellular space is more restricted due to both the cell membrane and the high macromolecule content. The rotational motion of hemoglobin molecules has been shown to slow down by a factor 2.2 in the erythrocytes compared to motion in a low concentration solution (Wang et al., 1997). This may arise either from higher intracellular viscosity or from obstruction by other Hb molecules. If one compares the rotational correlation times of Hb in solutions and intracellular Hb, the curves of correlation times versus concentration overlap (Lindstrom et al., 1976), suggesting that the concentration alone is responsible of this slower intracellular rotation. The ratio of intracellular and extracellular diffusion coefficients is clearly higher than two, a value as high as 8 has been reported (Blinc et al., 1990). If the average displacement of water molecules is studied for longer than a few milliseconds, the restriction induced by the cell membrane can be observed, resulting in apparently smaller intracellular diffusion coefficients

2.1.1.2 Hemoglobin

The maximal intracellular hemoglobin concentration, limited by hemoglobin-forming mechanisms, is 3.4 g Hb in 1 ml of cells. Indeed, the Hb concentration in normal adults is very close to this value. Hemoglobin is a large protein, with a molecular mass of 67 kD, and it fills one third of the erythrocyte volume. One erythrocyte carries over 100 million Hb molecules. The globin part of the molecule consists of four polypeptide chains (two alpha and two beta chains), each attached to an iron-containing heme moiety. Each heme can bind to one molecule of oxygen. The adult form of hemoglobin is HbA. In a hereditary disorder called sickle cell anemia, part or all of the hemoglobin is of the form HbS. In HbS, a single amino acid alters the 3-D structure of the hemoglobin molecule in such a way that when deoxygenated, proteins polymerize and precipitate within the erythrocyte, leading to the characteristic sickle shape (Hoffman et al., 2000).

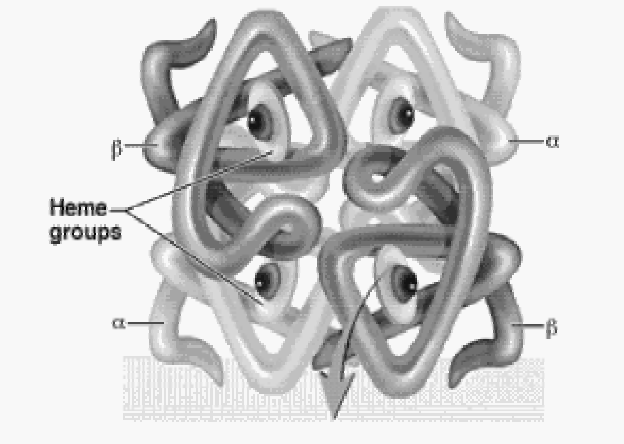

Figure 3

3D-rendered image of a hemoglobin molecule. The effect of deoxygenation on location of the heme is shown with an arrow. (Waters, 2002)

The presence of an oxygen molecule on the heme effects the electron configuration of Hb. In deoxygenated Hb, the iron atom in the heme is in a high-spin state (S=2), with four unpaired electrons, and is raised above the porphyrin plane. Binding the oxygen switches the iron to a low-spin state, resulting in S=0 and the iron atom is lowered to the porphyrin plane. If the hemoglobin is oxidized, methemoglobin (metHb) is formed. In metHb, the electron configuration becomes more complex and S=5/2.

2.1.2 Delivery of oxygen: vascular function

The vascular system ensures the supply of oxygen and nutrients to all regions of the body. The structure of blood vessel varies according to the function. Arteries that carry blood to tissue are thick and muscular in order to maintain the blood pressure. Blood volume is regulated by the smooth muscle cells in the arterial wall; relaxation of these muscles is triggered by vasorelaxative agents, such as nitric oxide and the concentration of hydrogen ions. As arteries branch, the diameter decreases and vessels thinner than 200 μm are called arterioles (Guyton, 1986). The exchange of gases and other substances takes place predominantly in the capillary bed, even if some of the small arterioles may serve as capillaries (Intaglietta et al., 1996; Sharan et al., 1989). The capillary wall is thin and permeable to water and small molecules (Guyton, 1986). The oxygen saturation decreases exponentially as blood moves through the capillary bed. Veins have a larger diameter than arteries and the vessel wall is thinner and softer. A schematic drawing of the vascular network is presented in figure 4. In the normal physiological state, arterial oxygen saturation is close to 100 % and venous oxygenation varies between 60 and 70 %. The blood flow in the human brain is approximately 50 ml/min per 100g of tissue. In smaller animals, the flow level is generally higher, for instance in rats levels of 100 ml/100 g/min have been determined (Calamante et al., 1999).

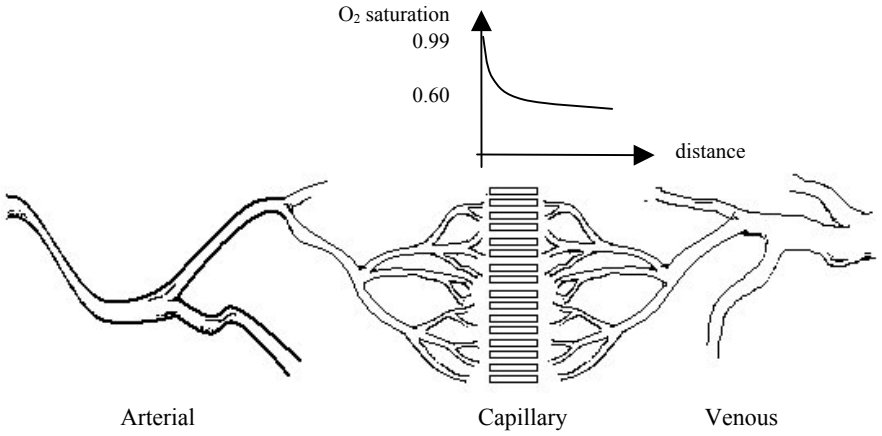

Figure 4: Vascular network

Cerebral blood volume and blood flow are very adaptive to changes in the demand for energy and oxygen. Neuronal activation increases the oxygen consumption, which is fulfilled by increasing the blood flow and blood volume. Depending on the stimulus and the brain region activated, flow increases by about 50 % and the volume by some 20 % (Moonen and Bandettini, 1999; Toga and Mazziotta, 1996). This process is not balanced but the demand for oxygen is overcompensated, resulting in higher venous oxygen saturation (Moonen and Bandettini, 1999; Toga and Mazziotta, 1996). In contrast, under low perfusion, such as when a feeding artery is obstructed, blood volume increases dramatically (Powers, 1991). In a serious hypoperfusion crisis, practically all of the oxygen is absorbed by the tissue, leading to highly deoxygenated venous blood (Ferrari et al., 1992; Sette et al., 1989).

Under normal function, relative changes in blood flow and volume are linked through the modified Grubb's law (Grubb et al., 1974; van Zijl et al., 1998):

$$\frac{CBV}{CBV_0} = \sqrt{\frac{CBF}{CBF_0}} \qquad \textbf{Equation 2}$$

In conditions with blood flow higher than 200 % of the physiological flow, the autoregulation fails and this relationship breaks down as the maximum dilatation capacity of the vessel walls is reached.

2.2 Nuclear magnetic resonance, NMR

NMR can be observed in all nuclei with unpaired protons and/or neutrons resulting in a non-zero spin quantum number I. The most typical nucleus in biomedical applications is hydrogen, ^{1}H (I = ½), as most tissue types consist mainly of water. Other interesting spin ½ nuclei are ^{13}C and ^{31}P but the NMR-sensitivity as well as the overall abundance of molecules containing these nuclei *in vivo* is much less than that of hydrogen, which is present in each water molecule as well as in most organic compounds.

2.2.1 Magnetization

When a non-zero nuclear spin is placed in an external magnetic field, the spin interacts with the field and the energy levels split to 2I+1 sublevels (Zeeman splitting), which is 2 for spin ½ nuclei. In thermal equilibrium, the lower level is slightly more populated. The ratio of spins is given by:

$$\frac{n_{-1/2}}{n_{1/2}} = e^{\frac{-h\gamma B_0}{2\pi kT}} = e^{\frac{-\Delta E}{kT}} \qquad \textbf{Equation 3}$$

This is the Boltzmann distribution where h (Planck constant), γ (gyromagnetic ratio) and k (Boltzmann constant) are constants, B_0 the external field strength, T temperature and ΔE the difference in energy between the states. The energy distribution can be perturbed by introducing energy quanta of size ΔE, which is equal to using electromagnetic radiation at frequency γB_0. In

practically all NMR systems, the frequencies are in the radio frequency (RF) range, from a few MHz up to 1 GHz.

In both energy states, the precession in B_0 occurs at the angular frequency $\omega_0 = 2\pi \gamma B_0$ (Larmor frequency), the lower state precesses around the positive and the higher state around the negative z-axis. In a system with many non-synchronized spins, average spin vector at xy-plane is zero while along B_0 there is a net vector M, called magnetization. This macroscopic quantity is a more heuristic measure than the quantum mechanical treatment of the spin distribution.

In the laboratory frame of reference, the magnetization in thermal equilibrium is usually chosen to be parallel to the positive z-axis. The manipulation of spin distribution by RF results in rotation of the magnetization towards the xy-plane and, if energy is still brought into the system, towards –z. The RF pulse synchronizes the spins, reaching the condition called phase coherence, and the resulting net transverse magnetization now rotates around z at the Larmor frequency. It is convenient to switch the coordinate system from the laboratory frame to frame rotating around z-axis at the Larmor frequency, so that the on-resonance transverse magnetization becomes stationary. Whenever there is net transverse magnetization in the xy-plan, the NMR signal can be detected through induction of current to an RF coil tuned to the frequency of the oscillation.

After the perturbation of the Boltzmann distribution, the thermal equilibrium in the spin system is recovered. This process is called NMR relaxation. In order to reach the equilibrium, the spins must release their excess energy to the surrounding medium, the lattice. Only systems oscillating at Larmor frequency are capable of absorbing this energy. The transverse magnetization in xy-plane disappears as spins lose their synchronization and disperse, the time constant of this dephasing process is called T_2* relaxation time. In this process, the net energy of the spin system remains the same. As relaxation rates ($R_i = 1/T_i$) are more convenient in quantitative models, these are often used instead of relaxation times.

The most significant type of interaction in NMR of spin ½ nuclei is magnetic dipole-dipole coupling between nuclear spins. In addition, the presence of paramagnetic molecules, with unpaired electrons, provides an efficient interaction pathway, as the magnetic moment of an electron is 657 times greater than the proton moment. Paramagnetic species both enhance relaxation and generate susceptibility shifts. In nuclei with I>½, there are additional relaxation pathways through quadrupolar interactions. In the following section, the presentation focuses exclusively on the proton (spin ½) relaxation.

2.2.2 Longitudinal relaxation: T_1 and $T_{1\rho}$

In longitudinal relaxation, water spins interact with the lattice, which in biological samples consists mainly of macromolecules, predominantly proteins. The interaction requires oscillation of the xy-component of the local field at the Larmor frequency, which can be provided through several mechanisms. Examples of such processes are thermal motion of proteins (rotation, translation, vibration) and exchange of protons and water molecules between free pool and the

hydration water layer of the protein. A convenient way to study relaxation in such an environment is to use distributions of frequency of the motion (Cowan, 1997):

$$J_m(\omega) = \int_0^\infty G_m(t)\exp(i\omega t)dt \qquad \textbf{Equation 4}$$

where $G_m(t)$ is the time autocorrelation function for the interaction of interest. The index m corresponds to different transitions between energy states. For rotational motion, the correlation function is exponential and the same is usually assumed for most relaxation processes. In this case,

$$J(\omega) \propto \frac{\tau_c}{1+\tau_c{}^2\omega^2} \qquad \textbf{Equation 5}$$

where τ_c is the correlation time of the motion; the time in which the motional state of the system changes significantly or, in other words, the autocorrelation function decays to 1/e of its initial value. In rotational motion, the interpretation of τ_c is straightforward: τ_c is approximately the time it takes to rotate an angle of one radian. The correlation times of different processes vary over a wide range. In pure water, the intramolecular correlation time is a few picoseconds while some of the proton exchange processes take place in time scale of seconds. Most of the protein hydration water exchanges in a nano-to-millisecond range, depending on the chemical interaction (Bryant, 1996; Koenig, 1999).

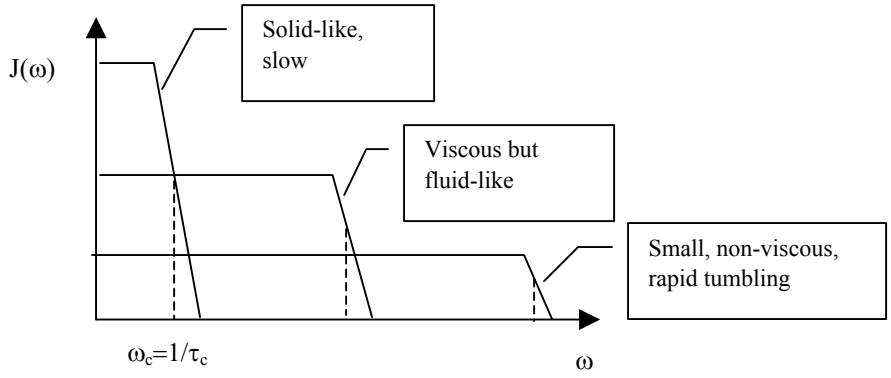

Figure 5: A schematic illustration of spectral densities for three different types of molecules. Frequencies corresponding to correlation times at the inflection points of the curves are shown with dashed lines.

In the general case, longitudinal relaxation depends on both J_1 and J_2:

$$R_1 = K\left[J_1(\omega_0) + 4J_2(2\omega_0)\right] \qquad \textbf{Equation 6}$$

This can be shown to give

$$R_1 = K\left[\frac{2/3\,\tau_c}{1+\omega_0{}^2\tau_c{}^2} + \frac{8/3\,\tau_c}{1+4\omega_0{}^2\tau_c{}^2}\right] \qquad \textbf{Equation 7}$$

where K is a constant, containing information of the magnitude of field fluctuation. It should be pointed out that these results are based on a rotational diffusion model (Cowan, 1997). When the system is far from condition $\omega\tau_c=1$, or the motional state differs greatly from rotation, this model is not appropriate and spectral densities are no longer Lorentzian. In such cases, the relaxation will often differ from exponential behavior.

2.2.2.1 Relaxation in the rotating frame

If spins are excited to the xy-plane and an RF pulse at the Larmor frequency, now parallel to magnetization is applied, spins cannot dephase and relax along the field generated by RF, of amplitude $B_1 = \gamma\omega_1$. This method is termed on-resonance spin lock. Alternatively, the spin lock can be delivered off resonance (with a shift from resonance $\Delta\omega$) and the relaxation occurs along effective field ω_{eff}

$$\omega_{eff} = \sqrt{\omega_1{}^2 + \Delta\omega^2} \qquad \textbf{Equation 8}$$

Typically, the spin locking field strengths are a few Gauss ($1G=10^{-4}$ T), in contrast to typical B_0 values of a few Teslas. In principle, the relaxation process in the rotating frame equals to T_1 relaxation at low B_0. However, the method itself carries in some aspects, related to the homogeneity of the sample and B_1 (Engelhardt and Johnson, 1996). In order to maintain the spin lock, the adiabatic condition must prevail, so that the effective field is larger than the rate of change in the orientation of the B_1 field. At a susceptibility interface, this condition may be violated for some spins and these spins start to experience transverse relaxation effects in the presence of an RF field. This may induce a dependency on B_0 into $R_{1\rho}$ relaxation (at constant B_1) as the susceptibility-related issues scale linearly with B_0. Unlike in the case of R_1, the increasing main field strength accelerates the apparent $R_{1\rho}$ relaxation (Engelhardt and Johnson, 1996).

In the presence of an RF field the longitudinal relaxation rate resulting from rotational motion is written as

$$R_{1\rho} = \frac{1}{2}K\left[3J_0(2\omega_1) + 5J_1(\omega_0) + 2J_2(2\omega_0)\right] \qquad \textbf{Equation 9}$$

In spin lock experiments, only ω_1 is varied and the dependence of $R_{1\rho}$ on ω_1 can be written as

$$R_{1\rho} = R_{1\rho}(\omega_1 \to \infty) + \frac{B}{1 + 4\omega_1^{\,2}\tau_c^{\,2}} \qquad \textbf{Equation 10}$$

where $R_{1\rho,0}$ and B are ω_1-independent constants. $R_{1\rho,0}$ is the baseline relaxation rate at high B_1, containing the contribution from B_0 while B, the dispersion amplitude, describes the strength of the effect of B_1. B also contains the correlation time, as can be seen from equation 5.

2.2.2.2 Protein solutions: NMR dispersion

As the relaxation rates depend on the ratio between the Larmor frequency (or, in the case of rotating frame, the frequency of the spin locking field) and the correlation time, it is useful to study the relaxation as a function of either B_0 or B_1. This is called NMR dispersion, NMRD (Hallenga and Koenig, 1976; Knispel et al., 1974; Koenig and Schillinger, 1969). Typically, NMRD profiles follow the spectral density functions. In a simple system with only one (rotational) correlation time, the NMRD profile is Lorentzian (Koenig et al., 1993) and the determination of the correlation time from the inflection point of the profile is straightforward. However, biological samples are nearly always far from simple and result in complex and often non-Lorentzian profiles.

The presence of proteins in a water solution induces significant relaxation enhancement, much more than their concentration alone would suggest. Thus, there must be some interaction between water and the macromolecule pool and a natural pathway for this would be the interaction between the protein body and its hydration water. On the other hand, it has been shown that only a relatively small, slowly exchanging fraction of hydration water actually contributes to the relaxation (Eisenstadt, 1985; Koenig et al., 1993). In general, the main pathways for the exchange of magnetization between the protein and bulk water can be divided into three categories. The first one involves exchange of water, either on the hydration layer (Andrasko, 1975; Koenig and Brown III, 1994) or to specific binding sites (Chopra et al., 1984; Venu et al., 1997). The second category is related to the exchange of protons of NH- and OH-groups (Duvvuri et al., 2001; Mäkelä et al., 2001; Thompson et al., 1973) and amides. The third mechanism is diffusion-mediated magnetization exchange, without any particle exchange. The importance of these contributions varies according to protein structure and mobility (Venu et al., 1997) and physical conditions (pH, temperature). Comprehensive reviews of different mechanisms involved in NMRD and longitudinal relaxation in protein solutions and in biological samples in general have been provided by Bottomley (Bottomley et al., 1984) and Bryant (Bryant, 1996).

The key factor affecting NMRD is the correlation time. It depends on molecule size (Menon and Allen, 1990), temperature and viscosity of the medium. Proton exchange is strongly pH-dependent (Wüthrich, 1986), with the exchange being catalyzed under alkaline (at physiological range) as well as under very acidic conditions. High concentration decreases correlation times (Lindstrom et al., 1976). The NMRD profiles of liquid protein profiles are typically Lorentzian (Koenig et al., 1993; Koenig et al., 1993). This refers to relatively free and rapid motion, which agrees with measurements of correlation times. In solutions of mobile proteins, the main relaxation mechanisms are exchange of both buried water and protons, the contributions being

nearly equal at pH around 7 (Venu et al., 1997). If the protein structure becomes rigid, as when it is chemically cross-linked, the motion slows down and relaxation is greatly enhanced (Koenig et al., 1993). Immobile proteins show solid-like intramolecular relaxation and their NMRD profiles are no longer Lorentzian, as the plateau at low frequency apparently disappears (Koenig et al., 1993). In such a case, the relaxation dispersion can be described using the so-called power law (Bottomley et al., 1984; Bryant, 1996), arising from protein backbone fluctuations (Korb and Bryant, 2001; Nusser and Kimmich, 1990)

$$R_1 = A\omega^{-B} + C \qquad \textbf{Equation 11}$$

in which A is a scaling constant, C the high-field relaxation rate and the factor B achieves values between 0.5 and 0.8. In samples of dry protein, B is high whereas in hydrated solutions, it approaches the value of 0.5. Interestingly, it was recently demonstrated that also partially hydrated immobile protein solutions show a plateau at low frequencies, due to the cross-relaxation between water and solid protein (Korb and Bryant, 2002). The dispersion in most tissue types resembles closely that observed in wet immobile protein solutions (Bottomley et al., 1984; Korb and Bryant, 2002).

*2.2.3 Transverse relaxation: T_2 and T_2**

Transverse magnetization decays as the phase coherence of spins decreases after excitation. This results from spin-spin energy exchange, which does not change the net energy of the system and thus does not require on-resonance oscillations. In terms of the net magnetization vector, R_2* can be described as the divergence of phases of individual spins (Fig. 6). As the phase distribution approaches a random distribution, the net transverse magnetization disappears at the rate R_2*. If a refocusing pulse is applied at time $\tau/2$, the phase distribution is inverted and, if the environment remains similar for each spin, the magnetization is restored at time point τ (Fig. 7). In multiecho sequences, the spins are allowed to dephase and are refocused again by applying more pulses at times $3\tau/2$, $5\tau/2$ etc. The most common multiecho sequence is that developed by Carr, Purcell, Meiboom and Gill (CPMG). In practice, there is always some signal loss and the rate of this decay is R_2. R_2* depends on both static and varying field fluctuation, whereas for R_2, the static and slowly varying effects are canceled; so R_2* cannot be lower than R_2. The contributions from these nearly static and varying phenomena can be expressed

$$R_2^* = R_2 + R_2' \qquad \textbf{Equation 12}$$

in which R_2‘ is the contribution from static field inhomogeneities that can be canceled by the refocusing pulse.

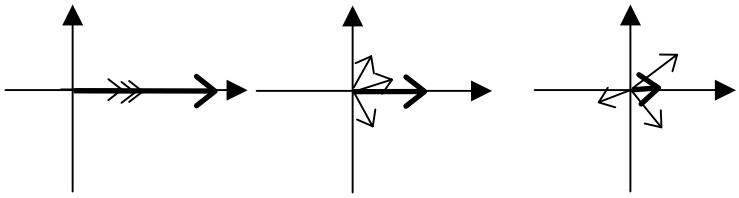

Figure 6: Dephasing of spins, resulting in zero net magnetization in the xy-plane (thick arrow) when the orientations of individual spins (thin arrows) are random. The rate of the signal loss is given by R_2*

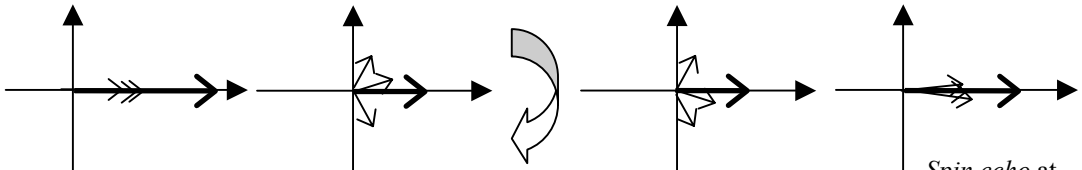

Figure 7: Effect of a refocusing pulse: R_2* effects are canceled. However, some magnetization is lost due to R_2 relaxation.

The loss of phase coherence results when the Larmor frequency in the system varies for an individual spin during the time τ. Temporal variation is induced by motion of other molecules, mainly macromolecules as they tumble due to thermal motion. Spatial variation is important as the water molecules diffuse in their environment. All these processes depend on the physical conditions of the system, such as temperature, viscosity and on the structure of the macromolecules, determining their motional state. If there are objects containing material of different susceptibility in the system, then stronger magnetic field gradients will be created. These gradients depend in size and shape on the geometry and orientation of the object. Diffusion of water in these gradients enhances the apparent transverse relaxation. In addition, exchange of either water or protons across a susceptibility interface enhances transverse relaxation, as the relaxation of spins within the macromolecule or a paramagnetic particle, is very fast.

The effect of these field fluctuations depends not only on the amplitude of the fluctuation but also on the time scale. Very slow phenomena can be effectively refocused, on the other hand, sufficiently fast changes are averaged over the experiment, a condition called motional narrowing. In terms of spectral densities, R_2 is given by

$$R_2 = \frac{1}{2}K\left[3J_0(0) + 5J_1(\omega_0) + 2J_2(2\omega_0)\right] \qquad \textbf{Equation 13}$$

yielding

$$R_2 = K\left[\tau_c + \frac{5/3\,\tau_c}{1+\omega_0{}^2\tau_c{}^2} + \frac{2/3\,\tau_c}{1+4\omega_0{}^2\tau_c{}^2}\right] \qquad \textbf{Equation 14}$$

Factor K is the same constant as in equation 7, containing information about local field variation. This equation describes the intrinsic ($\tau \to 0$) R_2 under a single source of fluctuation (one correlation time) and is usually too general for practical applications *in vivo*.

Longitudinal relaxation is naturally the absolute baseline for observed transverse relaxation. Indeed, it has been shown that the zero-field asymptote of $R_{1\rho}$ approaches the intrinsic R_2 (Santyr et al., 1988). As the refocusing interval is increased, dephasing mechanisms start to come into play and R_2 increases. Such mechanisms exist in pure water, due to coupling between protons and residual ^{17}O, but in the presence of different kinds of inhomogeneities, transverse relaxation is greatly enhanced.

When describing relaxation in the presence of paramagnetic inhomogeneities, a convenient choice of view is to study water molecules in the neighborhood of a paramagnetic object. One approach is to use numerical methods, such as Monte Carlo simulations to study the signal behavior in systems containing magnetic particles (Hardy and Henkelman, 1991; Weisskoff et al., 1994) or capillary-size cylinders (Boxerman et al., 1995; Fujita, 2001; Kennan et al., 1994). In analytical approaches, the space around the paramagnetic particle can be divided to subregions, each with their own characteristic relaxation properties. The inner sphere theory deals with spins during the time they are bound to the paramagnetic particle (Gillis et al., 1999; Gueron, 1975). In the outer sphere, the relaxation is governed by diffusion in field gradients around the object (Gillis and Koenig, 1987; Gillis et al., 2002; Gillis et al., 1999; Koenig and Kellar, 1995; Roch and Muller, 1999). This region can further be described by a fast dephasing region (called static dephasing region (Brown, 1961; Yablonskiy and Haacke, 1994) or "stormy gradient seas", (Brooks, 2002)), in which refocusing is very inefficient, and a slowly varying region ("islands of tranquility", (Brooks, 2002)), where most of the signal is rescued by the refocusing pulse. Interestingly, it seems that the relaxation in the outer sphere can be treated analogously to a two-site exchange process, if these two regions are treated as the exchanging sites (Brooks, 2002), although this neglects the intermediate region between these two extremities. The contribution of these regions to apparent relaxation rate depends on the degree of the susceptibility shift as well as on the dimensions and motional state of the system. In figure 8, relaxation due to susceptibility variation is presented as a function of the size of the spherical inhomogeneity (Weisskoff et al., 1994).

Relaxation under weak magnetic inhomogeneities has been treated in several models, as it is of obvious interest *in vivo*. Yablonskiy and Haacke presented the "static dephasing regime" theory in 1994 (Yablonskiy and Haacke, 1994), Jensen and Chandra their "weak diffusion theory" in 2000 (Jensen and Chandra, 2000), and Kiselev and Posse their model for dephasing in the cerebrovascular network in 1998-1999 (Kiselev and Posse, 1999; Kiselev and Posse, 1998). The conditions for weak magnetic treatment vary slightly according to the authors, but in general it is required that the magnetic field varies little during the refocusing interval ($\Delta\omega\tau_{CPMG}<1$). It has

also been shown that the fast chemical exchange model (which will be discussed in more detail in the next chapter) can be applied both to the inner and outer sphere relaxation (Brooks et al., 2001) both at the long echo limit (motion of water is fast compared to refocusing time, resulting in motional averaging) and at the short echo limit (effective refocusing). In the case of diffusion among spherical inhomogeneities, the parameters of exchange theory were connected to diffusion-related parameters. The exchange time reflects one quarter of the time to diffuse past the particle and the volume fraction in exchange equation reflects a compartment 1.7 times the volume fraction of the particles.

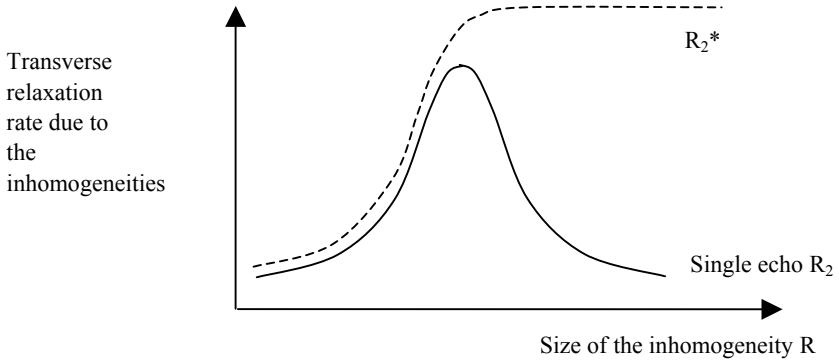

Figure 8: A schematic drawing of the transverse relaxation as a function of the size of the inhomogeneity (Weisskoff et al., 1994). With small particles, or fast diffusion, motional narrowing decreases both R_2 and R_2*. When the particle size increases, field gradients become smoother and can be more efficiently refocused.

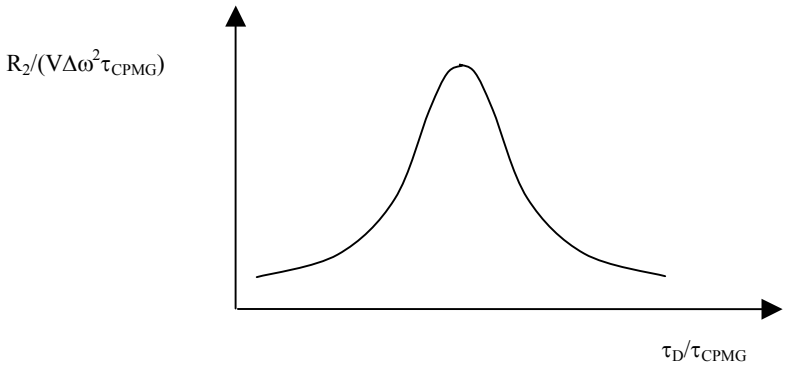

Figure 9: If a CPMG sequence is used in the case of weak magnetic inhomogeneities, the peak in normalized R_2 occurs close to the point where diffusion time (R^2/D, R is the effective radius of the particle and D is the diffusion coefficient) equals the refocusing interval (Brooks et al., 2001). On the left hand side (long-echo limit), the dephasing is very fast, resulting in motional averaging, while on the right hand side (short-echo limit), the refocusing is efficient since only a part of the field variation is experienced by the spins between the refocusing pulses.

2.2.4 Multiple compartments and exchange

In typical biological samples, several sites for water exist and often the relaxation rates in these sites differ. Usually there are susceptibility differences between dia- and paramagnetic sites and also from one diamagnetic compartment to another. The effect on the measured apparent relaxation rate depends on the time scale of the mixing of these compartments. If the mixing is very slow, the observed signal is a sum of signals from these compartments, weighted with corresponding water fractions (Zimmermann and Brittin, 1957):

$$S(t) = \sum_i p_i \exp(-R_{2,i} t) \qquad \textbf{Equation 15}$$

where p_i and $R_{2,i}$ are the weight and relaxation rate of i^{th} compartment. The observed signal decay is multiexponential, even if in practice, some compartments may not be visible due to the chosen experimental time scale.

The other extreme case is very fast exchange. In this case, most water molecules probe all compartments during the experiment and relaxation rates are averaged (Zimmermann and Brittin, 1957).

$$R_2 = \sum_i p_i R_{2,i} \qquad \textbf{Equation 16}$$

This is a very simplified view, neglecting the effect of water motion during the experiments as well as the possible susceptibility difference between the sites. A more realistic model for relaxation in systems with exchanging sites of different Larmor frequencies was presented in 1963, when Luz and Meiboom [Luz Z, 1963 #162] derived the equation (which in the following text will be referred to as the LM equation) for CPMG R_2 under multi-site chemical exchange

$$R_2(g) = R_{2,0} + \left(1 - 2\tau_c g \tanh(2\tau_c g t)^{-1}\right)\tau_c \sum_i p_i \delta_i \qquad \textbf{Equation 17}$$

in which g is the refocusing rate, t_c the correlation (exchange) time and p_i and δ_i the weight and frequency shifts in i^{th} compartment. $R_{2,0}$ is the baseline relaxation rate at infinitely fast refocusing, with no effect from dephasing of the spins and can be expressed as a volume-weighted sum of relaxation in the compartments (Equation 15). The equation was derived under the assumption of fast exchange, in which the exchange rate is much higher than the frequency shifts and relaxation is slow compared to the refocusing rate. One year later, Allerhand and Gutowsky showed that the theory could be applied even if some of the criteria for fast exchange did not hold (Allerhand and Gutowsky, 1964). Intermediate exchange, i.e. the region where the frequency shifts, relaxation times and pulse spacing are in the same range, is more complex to model analytically (Davis et al., 1994; Ishima and Torchia, 1999; Jen, 1978; Kaplan, 1980; Millet et al., 2000). These models deal in principle with the same parameters as the LM equation, but the different contributions (baseline, dispersion amplitude) cannot be separated as easily as in LM. In a simple, chemically exchanging system of water, enriched to 4 % in ^{17}O, the correlation times obtained from Lorentzian fits of $R_{1\rho}$ data and LM fits of R_2 data agree (Knispel and Pintar, 1975).

In spectra, non-exchanging species show separate peaks, each at their Larmor frequency. As exchange rates increase, the peaks start to overlap and in the case of fast exchange, only one peak is detected at frequency equal to the weighted sum of the individual frequencies.

2.2.5 Spectroscopy and imaging

In NMR spectroscopy the induction signal is measured as a function of time (FID: free induction decay). Fourier transform reveals the frequency distribution of the data. In biological samples, the most dominant peak in the proton spectrum comes from water. After water suppression, signals from some other molecules containing hydrogen can be seen. The signal induced in the coil comes from NMR-visible protons in all the material the coil can see. In some cases, this is desired but often selection of a volume of interest is needed. The simplest method is to saturate slabs around the desired volume (outer volume suppression, OVS) (de Certaines et al., 1992). More sophisticated volume selection methods are based on the selective refocusing of the volume of interest; an example of such a method is the image-selected *in* vivo spectroscopy (ISIS) (Ordidge et al., 1985).

In imaging, the slice is chosen with a frequency-selective RF pulse and a gradient set perpendicular to the slice. The frequency and phase of the spin in the slice are encoded and a 2-dimensional Fourier transform results in an image in the spatial coordinates. Normally, the water signal dominates the image contrast. In spectroscopic imaging, a spectrum is acquired from each voxel, now localized with a combination of two or three phase encoding gradients, and images of different NMR-visible molecules can be constructed. As the concentration of these molecules *in vivo* is much lower than that of water, the quality and resolution of spectroscopic images is poorer than the quality of normal MRI images.

Using conventional imaging sequences, each phase step is carried out separately, which is time consuming. The use of fast sequences solves this problem but introduces other limitations, for instance in the minimum echo time. If 2-dimensional data is not required, acquiring a profile or a line scan is sufficient, saving time.

2.2.6 Measurement of relaxation times

2.2.6.1 T_1 and $T_{1\rho}$

The traditional way of measuring longitudinal relaxation is to use inversion recovery sequences. The magnetization is inverted to –z and allowed to relax for time TI (inversion time). After this, magnetization is rotated to the xy-plane and measured. In spectroscopic sequences, a single 90-degree pulse is generally utilized; in imaging a spin echo acquisition is often used. The signal behavior as a function of TI is given

$$S(TI) = S(\text{infinity})(1 - k\exp(-R_1 TI)) \qquad \textbf{Equation 18}$$

Ideally k=2 but in practice pulse imperfections and other experimental shortcomings effect and typically $k \approx 1.95$. Another way to determine R_1 is to acquire data with different repetition times (TR). Now, as the inversion pulse is replaced by a 90-degree pulse, the factor k in Equation 16 is close to unity and the time parameter is TR instead of TI. This method is called the saturation recovery and it is generally more inaccurate, as the dynamic range is smaller. However, it is less time consuming than the inversion recovery method, because the TRs are shorter (de Certaines

et al., 1992). The third way of determining R_1 is to detect the recovery curve using several small-angle read-out pulses (Brix et al., 1990; Look and Locker, 1970).

In the measurement of $T_{1\rho}$, the longitudinal relaxation in the rotating frame, spins are tilted to the xy-plane and a constant RF pulse is applied locking the spins to precession around the applied field. The signal as a function of spin lock time (TSL) is expressed as

$$S(TI) = S(0)\exp(-R_{1\rho}TSL) \qquad \textbf{Equation 19}$$

The amplitude of the spin locking field (B_1) is usually determined by studying the time required to invert the spins using certain pulse amplitude. This holds for on-resonance spin locking. If the field is applied off-resonance, the effective spin locking field is given by Equation 8.

2.2.6.2 T_2* and T_2

The most straightforward way to determine T_2* is to study the decay of an FID or the line width of the water peak in the spectrum. In imaging applications, the signal resulting from a single excitation can be collected using a gradient pulse and T_2* is the time constant of the signal decay as a function of the delay between excitation and the gradient echo (time to echo, TE).

For determination of T_2, a refocusing pulse must be applied. In single echo experiments (often called Hahn echoes) one refocusing pulse in applied at time $\tau/2$ and the echo at τ is detected, TE equals τ. The relaxation time is determined using several τ-times. When measuring systems with strongly τ–dependent relaxation, single echoes are not optimal, as the contribution of τ–dependent phenomena is different at each TE. In such cases, the multiecho sequence is more unambiguous. Instead of measuring the first echo, the signal at τ is allowed to dephase again and another refocusing pulse is applied at 1.5 τ, and this is continued until the desired echo is measured at TE=nτ, n is the number of refocusing pulses. To avoid cumulative errors in pulse accuracy, the phase of refocusing pulses is usually cycled (de Certaines et al., 1992). One frequently used multiecho sequence is the modification devised by Meiboom and Gill of the original sequence by Carr and Purcell (de Certaines et al., 1992).

2.3 NMR of blood

2.3.1 NMR properties of blood

From an NMR point of view, blood differs from other protein solutions in certain ways. First, in blood, erythrocytes and plasma form a two–compartment system, with a high protein content within the cells and a lower protein content in plasma. The other special feature in blood is the magnetic susceptibility of hemoglobin protein, i.e. its diamagnetic nature in oxygenated state and moderately paramagnetic properties in deoxygenated state (Pauling and Coryell, 1936). This both affects directly the relaxation properties of hemoglobin molecules and creates a susceptibility shift between the intra- and extracellular spaces (Fabry and San George, 1983; Thulborn et al., 1982). By using oxidizing agents, such as $NaNO_2$, hemoglobin in cells can be converted to methemoglobin. MetHb remains paramagnetic regardless of the blood oxygenation level.

Across the cell membrane there is a sudden shift in susceptibility. This shift has been measured in several experiments, using CPMG data and the Luz-Meiboom equation (Bryant et al., 1990; Gillis et al., 1995; Meyer et al., 1995; Thulborn et al., 1982) as well as using other methods, such as the frequency shift-based methods (Spees et al., 2001; Weisskoff and Kiihne, 1992) or non-NMR methods (Alpert and Banerjee, 1975; Cerdonio et al., 1978). There is some variation in the presented values, but most reports estimate the intra-to-extracellular susceptibility shift to be 0.2-0.4 ppm in fully deoxygenated blood.

As the magnetic field changes accordingly, there must be field gradients near the cell membrane. These gradients depend on cell shape and its orientation to the main field B_0. The perturbation of the main field in point **r**, inside or outside the cell, can be calculated by solving the Biot-Savart law (Gillis et al., 1995),

$$\Delta\mathbf{B}(\mathbf{r}) = \frac{\chi}{4\pi}\int_S \frac{\mathbf{B_0}\times\mathbf{n}\times(\mathbf{r}-\mathbf{R})}{|\mathbf{r}-\mathbf{R}|^3}\,dS(\mathbf{R}) \qquad \textbf{Equation 20}$$

in which χ is the intracellular susceptibility. The integration is performed over the erythrocyte surface S, **n** is the normal of the surface at point **R**. The dependence on cell orientation comes through the cross product between main field $\mathbf{B_0}$ and **n**.

2.3.2 NMR of hemoglobin

NMR field dispersion in Hb solutions has been measured by several groups. Lahajnar et al. (Lahajnar et al., 1976) measured R_1 of fluoromethemoglobin solutions in the range 2-100 MHz and the observed correlation time of 0.9 ns was attributed to Fe^{3+} electron spin relaxation time. Lindstrom et al (Lindstrom et al., 1976) studied normal and sickled Hb solutions and cells and reported correlation times around 100 ns for Hb solutions at concentrations similar to intracellular Hb concentration. In addition, a strong dependency of correlation time on Hb concentration was evident, especially when the intracellular concentration was exceeded. In the work of Eisenstadt (Eisenstadt, 1985) the dispersion of both R_1 and R_2 were studied in detail. A distribution of R_2 values was observed and this distribution was enhanced upon denaturation. R_1 was found to follow two-site exchange formalism, which did not hold for R_2. However, no definitive conclusions with regard to the contribution of different relaxation mechanisms could be drawn.

Cameron et al (Cameron et al., 1988) studied the gradual dehydration of aqueous Hb and its effect on Hb R_1. The linear subregions in the T_1 vs. concentration curve were attributed to water compartments of different mobility and the degree of freedom. They also determined values of T_2 (single echo, TE 1-30 ms) and found a biexponential decay, with T_2 components of 5 ms and 10-50 ms. The shorter component was independent of the Hb concentration while the longer component correlated positively with the Hb content. A comparison of rotational correlation times in intracellular space and in a water solution was carried out by Wang et al. (Wang et al., 1997). They observed over two-fold slowing down so that the observed τ_c was 84 $*10^{-9}$ s in

cells and 38 $*10^{-9}$ s in solution. The ratio of intra- and extracellular diffusion coefficients has been determined by Blinc et al (Blinc et al., 1990) reporting $D_{in}/ D_{out} = 8$.

2.3.3 Longitudinal relaxation in blood

The studies of longitudinal relaxation in blood have concentrated on NMRD experiments, both using a relaxometer and through spin-lock experiments. A review of early experiments was provided by Brooks et al. in 1975 (Brooks et al., 1975). It was noted that in most previous experiments, as well as in their data, that the R_1 decay was very close to a single exponential. The authors applied a simple fast exchange theory to their R_1 data with satisfactory results. A relaxation enhancing effect of increasing pH was observed throughout the B_0 range from 0.02 to 6 MHz, the magnitude was reported to be about 25% per pH unit. Lindstrom et al (Lindstrom et al., 1976) reported correlation times of 200 ns for normal blood and 300-600 ns for sickle cell blood. This difference was attributed to aggregation of HbS, resulting in slower motion. Zipp et al (Zipp et al., 1977) measured $R_{1\rho}$ (B_1 from 0 to 7 G) packed normal and sickle cells and reported correlation times of 10 μs for sickle cells, but observed no dispersion in packed normal cells. Koenig and Brown (Koenig and Brown, 1984) measured NMRD in rabbit blood and stated that unlike most other tissues, blood dispersion resembled the behavior of a cell-free, mobile protein solution rather than the characteristics seen in immobilized systems.

Eisenstadt and Fabry varied the intracellular Hb concentration by osmolarity and determined relaxation rates of hemoglobin molecules (Eisenstadt and Fabry, 1978). A relatively low, apparently single component R_1 and a high, multicomponent transverse (CPMG) rate were found. Cameron et al (Cameron et al., 1988) compared $R_{1\rho}$ (B_1=1kHz, B_0 7T) in whole blood, packed cells and disrupted packed cells. Interestingly, they found the highest relaxation rates in whole blood (27 1/s), and in packed cells (22 1/s). After disruption, the rates decreased to 9 1/s. The oxygenation of these samples was not reported. Sullivan et al (Sullivan et al., 1988), Bryant et al (Bryant et al., 1990) and Spees et al. (Spees et al., 2001) observed a distinctly linear dependence on hematocrit over a broad Hct range in whole blood.

The dependence of R_1 on oxygenation has not been studied in detail. In reports by Thulborn et al (Thulborn et al., 1982) and Gomori (Gomori et al., 1987) graphical data of R_1-BOLD is provided but due to scaling issues, no possible effect can be visually detected. It has also been explicitly stated that blood R_1 at 1.5 T and 4.7 T is independent of oxygenation (Atalay et al., 1995; Spees et al., 2001). In the paper by Bryant et al. (Bryant et al., 1990) the possibility of small relaxation enhancement by deoxygenation is discussed.

2.3.4 Transverse relaxation in blood

During 1990's, the interest in transverse relaxation in blood increased greatly as fMRI based on the BOLD effect (Ogawa et al., 1992) was established (Bandettini et al., 1992; Frahm et al., 1994; Kwong et al., 1992). As more quantitative models for physiological changes were created, the need for understanding blood NMR became evident. Most of the theoretical work has been carried out on R_2, the few existing reports on R_2* tend to be rather descriptive. The studies of R_2 can be roughly divided into two categories: dependence of R_2 on CPMG echo

spacing and its relationship to water motion and dephasing effects and, as a second and perhaps more empirical line of research, modeling of blood oxygenation level dependence, BOLD.

2.3.4.1 Mechanistic studies

The discussion on erythrocytes and relaxation started in the 70's when Brindle et al. noted the susceptibility issues related to erythrocytes and blood oxygenation (Brindle et al., 1979). The earliest reports on blood T_2 are from the 80's. Fabry and San George (Fabry and San George, 1983) gave their warning on line broadening in solutions of deoxygenated erythrocytes and in 1982, the fundamental work by Thulborn was published (Thulborn et al., 1982). In that paper, the Luz-Meiboom equation was applied to blood CPMG relaxation data for the first time in the form:

$$R_2(g) = R_{2,0} + p_{ery}(1-p_{ery})\Delta\omega\tau_{exch}\left(1-2\tau_{exch}g\tanh(\tau_{exch}g)^{-1}\right) \qquad \textbf{Equation 21}$$

in which $R_{2,0}$ is the intrinsic relaxation rate at infinitely fast refocusing, $\Delta\omega$ the oxygenation-dependent susceptibility difference between erythrocytes and plasma and t_{exch}, the exchange time between the compartments in the original LM, is now interpreted as the correlation time of the dephasing process. g is the rate of refocusing, $1/\tau_{CPMG}$. The relative sizes of the compartment (p_{ery} and 1- p_{ery}) are often replaced by hematocrit and 1- hematocrit, even if the smaller water content in erythrocytes introduces some bias.

The resulting 0.6 ms correlation time at 4.3 T was attributed to intracellular diffusion. In addition, relaxation as a function of hematocrit was measured and also BOLD behavior was demonstrated. Brown et al. confirmed the importance of susceptibility-induced field gradients in transverse relaxation (Brown, 1983). These studies were followed by the work of Gomori et al. (Gomori et al., 1987), where they found longer correlation times at low field (9.1 ms at 0.71 and 0.4 T) and, since these times are close to exchange time across the cell membrane, these workers proposed the transmembrane exchange as a low-field relaxation mechanism. Gillis and Koenig (Gillis and Koenig, 1987) and Brooks et al (Brooks et al., 1989) discussed the origin of the field gradients and concluded that both intra- and extracellular gradients participate in the dephasing process. Other reports, giving mainly sparse values of blood relaxation rates as side products of other studies, have been published by a few groups (Hayman et al., 1988; Nummi et al., 1986).

In 1990, several interesting papers were published. Bryant et al studied the dependence of CPMG-R_2 on hematocrit and on echo spacing (Bryant et al., 1990). Linear hematocrit dependence was found and the correlation time from an LM fit was 10 ms at 1.4 T. The dramatic decrease in dependence on echo spacing in lysed cells was demonstrated. Santyr et al. (Santyr et al., 1990) compared the exchange and diffusion approaches and concluded that both of them satisfactorily described the relaxation processes within erythrocytes. Matwiyoff et al. analyzed the spectra of oxygenated, carbonated and deoxygenated hemoglobin and methemoglobin (Matwiyoff et al., 1990) by deconvolution into intracellular and extracellular signals. In their later work (Gasparovic and Matwiyoff, 1992), more vigorous modeling was applied and some experimental shortcomings were corrected for and the data reproduced.

However, the main conclusions remained the same: the main factor in line broadening upon deoxygenation was apparently diffusion. This convolution approach was disputed by Springer (Springer, 1994), based on the bulk magnetic susceptibility theory, predicting a powder-pattern spectrum from intracellular spins, instead of a separable line.

Meyer et al measured CPMG data at 4.7 T in 1995 (Meyer et al., 1995) and proposed proton exchange between cell water and OH groups in hemoglobin molecule to be the explanation for the determined 1.6 ms exchange time. In the work of Gillis et al., (Gillis et al., 1995) the field gradients of cells containing metHb were mathematically modeled and the signal behavior simulated using a random-walk method. The resulting dependence on CPMG echo spacing was indeed well characterized by the LM equation. The contributions from intra- and extracellular gradients were comparable, but the balance depended on the echo spacing. The correlation time for the diffusion process was found to be 2.0 ms at 4.7 T. Ye and Allen (Ye and Allen, 1995) chose a similar method, but a different model for the field gradients and water dynamics. Based on relaxation rate analysis of normal and spherical erythrocytes they concluded that the transmembrane exchange was detectable in LM fits of subtraction curves $R_{2,\,normal}$- $R_{2,\,spherical}$.

In 1998, two papers by the Toronto group were published (Li et al., 1998; Stanisz et al., 1998). They modeled blood as a 3-site system (erythrocytes, plasma and macromolecules) and employed CPMG- and diffusion sequences (Stanisz et al., 1998) or a hybrid of these two sequences (Li et al., 1998). The values for water residence times in erythrocytes derived using their model agreed well with literature data. In 2000, Jensen and Chandra (Jensen and Chandra, 2000) published an analytical model on blood relaxation in weak magnetic inhomogeneities and applied their theory to the data of Ye and Allen (Ye and Allen, 1995) and Brooks (Brooks et al., 1995). It was shown that the model provided better fits to the data than LM and it also defined the correlation time more precisely, now considered to represent the decay rate of the temporal correlation function. On the other hand, the difference between the models in whole blood data is not large and justifies the use of LM as a calibration curve. In addition, the correlation times derived using the theory are close to those given by LM.

2.3.4.2 BOLD characteristics: R_2 and R_2*

The LM equation contains information of blood oxygenation in the term $\Delta\omega$, as $\Delta\omega = B_o * \Delta\chi$(in ppm) (Brooks and Di Chiro, 1987), and this term is squared in LM. The quadratic dependence on blood deoxygenation has been observed in all reports on BOLD in isolated blood. The magnitudes of the non-constant terms depend on $\Delta\chi$, τ_c and τ_{CPMG}. If negligible frequency shift is assumed for oxygenated blood, there is no linear term.

In the work of Cottam and Waterman (Cottam and Waterman, 1976), T_2s of normal and sickle cells were measured as a function of their oxygenation. In sickle cells, the quadratic behavior was apparent, but in normal cells, T_2s actually shortened with increasing oxygenation. The behavior of sickle cells was attributed to the change in the motional state upon sickling, rather than to the paramagnetic properties of Hb. The data from normal cells was not discussed. The first systematic approach to model BOLD in whole blood was by Wright et al in 1991 (Wright et al., 1991). They studied human blood *in vitro* and *in vivo* at 1.5 T and determined R_2s using

four different values of τ_{CPMG}. By fitting baseline rate and the second order term as a function of deoxygenation, BOLD was well described at each τ_{CPMG}. 1997, Barth and Moser (Barth and Moser, 1997) published data on both R_2 and R_2* in blood, again at 1.5 T but now at room temperature. Also in this study, the model proposed by Wright was satisfactory. Li et al. measured R_2* in blood samples and *in vivo* (Li et al., 1998) using the signal from femoral artery and inferior vena cava. From the blood phantom data, oxygen extraction ratios were determined *in vivo*. In the blood samples, the quadratic behavior was evident and the whole second order polynomial was used in the fitting. The magnitude of the linear terms was small, suggesting that a fit similar to Wright's might have been nearly as good. *In vivo*, the values of R_2* were in the same range as *in vitro*, but now the second order term was not as dominating as *in vitro*, which may be just a coincidence, due to the lower signal-to-noise *in vivo*.

A thorough analysis of blood R_2 and R_2* *in vitro* was carried out by Spees et al 2001 (Spees et al., 2001). R_2 was determined using a CPMG sequence and R_2* was analyzed from the signal envelope of the last spin echo. The BOLD in both R_2 and R_2* was easily fitted to quadratic function. Contrary to other reports on gradient echo data, they found nonexponential signal decay in R_2*. In addition, the effect of deoxygenation on the relaxation rates in their study was more prominent than that reported earlier and the effect seen in our studies (**IV**).

In conclusion, the BOLD in both R_2 and R_2* follow quadratically the degree of deoxygenation. The steepness of this dependence is a function of field strength (through susceptibility), hematocrit (concentration of inhomogeneities) and sequence details (refocusing interval, CPMG vs. single echo).

2.4 fMRI

Currently, the term functional magnetic resonance imaging is usually associated with studies in which changes in blood oxygen saturation are used as a contrast mechanism to derive quantitative information of physiological parameters. A wider definition of fMRI includes also non-BOLD methods, mainly the measurement of blood flow through changes in apparent R_1 (Kwong et al., 1992) and "pseudo-diffusion constant", reflecting capillary blood flow (Henkelman et al., 1994; Le Bihan and Turner, 1992). Interestingly, it was observed recently that the cerebral diffusion coefficient dropped during visual activation (Darquie et al., 2001), in contrast to the situation with flow-mediated diffusion changes. This was attributed to transient swelling of neuronal and glial cells upon activation.

Typically, BOLD-fMRI is used to observe neuronal activation upon some external (visual, auditory, sensory etc) or internal (higher brain functions: memory, attention etc) stimulus. The stimulus induces an increase in oxygen consumption and, in a few seconds, an elevation of local CBV and CBF. In most brain regions, the hemodynamic changes overcompensate for the consumption, so the local oxygenation in veins increases which is observed as an increase in T_2- or T_2*-weighted signal or as longer relaxation times (Moonen and Bandettini, 1999; Toga and Mazziotta, 1996). If the BOLD behavior in blood or, alternatively, blood oxygenation, is known, then the changes in voxel R_2 can be used in the quantification of OER (Li et al., 1998; Oja et al., 1999; Wright et al., 1991) or blood volume (van Zijl et al., 1998).

The signal increase in BOLD-fMRI comes from two origins. First, elevated blood oxygenation decreases the transverse relaxation rate in blood and the susceptibility difference between blood and tissue, decreasing the extravascular field gradients. The effect on blood relaxation influences both T_2 and T_2*, but the extravascular effects are believed to be significant only in T_2* experiments (Ogawa and Lee, 1990). However, there are some reports on activation-induced relaxation changes in the extravascular space in the intracellular metabolite signal (Zhu and Chen, 2001). In T_2* experiments, approximately half of the signal change originates from intravascular spins. The second factor in the BOLD signal change is the effect of blood volume change. At typical imaging field strengths, relaxation in blood is less efficient than that occurring in tissue. As the observed signal is a blood volume–weighted average of signals coming from tissue and blood pools (van Zijl et al., 1998), an increase in blood volume leads to an increase in the net signal, even when the blood oxygenation remains constant. When moving to higher fields, the venous blood relaxation rate becomes closer to that in tissue and volume effects become less significant. Depending on the sequence details, already at 4.7 T, the baseline venous relaxation rate is very close to the tissue rate. At very high field and/or with very deoxygenated blood, increases in blood volume result in a decrease of the signal and observed relaxation rate.

The field dependence of the BOLD has been the subject of debate. The susceptibility shifts increase linearly with field strength (Brooks and Di Chiro, 1987) and R_2 and R_2* are a quadratic function of the shift. This predicts that there should be a major enhancement of BOLD at high field. However, the large intravascular BOLD effects are accompanied by a dramatic increase in blood relaxation rates. In the echo time region typical for imaging, this attenuates the signal arising from venous and even capillary vessels and thus the compartments with the largest signal changes become invisible. This diminishes the high field BOLD but the benefit is the better localization from veins (1.5 T (Frahm et al., 1994; Oja et al., 1999)) towards capillary region (4.7 T and higher (Lee et al., 1999; Ugurbil et al., 1999)).

In addition to changes related to transverse relaxation, increased blood flow has an influence on the apparent T_1 and thus the signal intensity also in T_2-weighted images. If the repetition time is relatively short, most spins in the imaging slice are saturated and the net signal is attenuated. However, blood flow brings new, non-saturated spins, which shortens the apparent T_1 of the blood (Lu et al., 2002). This is seen as a flow level dependent signal behavior in fMRI images.

The spins in the blood pool are exploited also in arterial spin labeling techniques (Detre and Alsop, 1999; Kwong et al., 1992; Silva and Kim, 1999; Williams et al., 1992; Wong et al., 1997). Blood spins are inverted in a separate slice, positioned usually in the neck of the subject, and the effect of the inflow of labeled spins on the signal in brain tissue is studied. With the application of certain assumptions, the blood flow rate can be derived. These models will be discussed in more detail in chapter 4.4.

3 AIMS OF THE STUDY

As blood is an important and dynamic constituent of living tissues as well as a source of the NMR signal, there is a clear need for description and understanding of NMR relaxation properties of blood. However, while some aspects of blood NMR have been described in a very elegant and thorough manner, other reports tend to treat the subject rather qualitatively. Often the data is acquired under non-physiologic conditions and the results cannot be applied *in vivo*.

The aim of the present study is to describe the blood relaxation as a function of both hematocrit and oxygen saturation, under physiological conditions. In addition to this calibration, the work attempts to explain these data in terms of relaxation mechanisms.

The specific aims are:

1) Quantification and interpretation of the effects of blood oxygen level on transverse (R_2, R_2*) and longitudinal (R_1, $R_{1\rho}$) relaxation in isolated blood.

2) The effect of hematocrit on blood relaxation parameters.

3) The effect of the determined dynamic properties of blood on *in vivo* quantitative fMRI.

4 MATERIALS AND METHODS

4.1 Blood samples and the setup for NMR of blood

The bovine blood was collected from a local slaughterhouse into beakers containing sodium citrate (final concentration 20 mM). The blood was stored at 4° and used within a week from delivery. During the storage time neither clotting nor hemolysis was detected and the concentration of methemoglobin did not change significantly. The human blood was tested donor blood from the blood bank. These samples were used within 48 hours from donation. The rat blood was collected by cardiac puncture into tubes containing sodium citrate.

The samples of whole blood of normal hematocrit were collected directly from agitated beakers. For samples of nonphysiological Hct, portions of plasma and cells, obtained by centrifuging the blood 15 min at 600 x g were mixed. Lysate was prepared by first removing the buffy coat, washing the cells with isotonic NaCl and adding distilled water to replace the removed plasma volume. This resulted in immediate cell lysis and the remaining ghosts were spun down for 30 min at 15 000 g. The net protein content was restored by adding BSA 6 % of the volume of distilled water. During the measurements, blood oxygenation level was monitored using blood gas analyzers (ABL-500, Radiometer Inc., Copenhagen, Denmark and i-STAT, i-STAT Co., East Windsor, NJ, USA). The hematocrit was detected either by using a blood gas analyzer (ABL-500) or from the volume fraction of centrifuged cells.

The blood samples were measured in a jacketed perfusion setup where the temperature in the sample tube inside the magnet was maintained at room temperature. The blood oxygenation was manipulated in a custom-built gas exchange chamber using gas mixtures of O_2 and N_2, both containing 5 % CO_2. In the tubings of low gas permeability, the oxygenation was very stable. To minimize the effect of possible small changes in Y, the order of data series in prolonged measurements (CPMG experiments in **II** and **III**) was randomized.

4.2 NMR methods and data analysis in blood measurements

4.2.1 Hardware and experimental setup

Experiments at 1.5 T were performed on a Philips ACS-NT, using a 100 mm surface coil receive and body coil transmit. The sample was positioned vertically and the coil was supported on the side of the sample tube.

The experiments at 4.7 T were performed on Varian ^{UNITY}Inova and GE Omega systems. In the experiments with the Varian system, a dual lobe surface coil was used and the sample tube was positioned inside the coil. In the experiments with GE, a solenoid coil was used. In both cases, the sample tube was aligned upright and perpendicular to magnetic field.

4.2.2 Determination of relaxation times

In all blood experiments, the shimming was done on oxygenated blood and kept unchanged throughout the whole experiment.

T_1 at 4.7 T was measured using an inversion recovery sequence (TIs from 500 to 2500 ms, TR 10 s). An adiabatic inversion pulse was used, followed by a single spin echo acquisition (TE 12 ms) from a 3 mm slice across the sample tube. The repetition time (TR) was 10 s. From the slice profile, points with intensities higher than 50 % of the maximum at long TI were summed and these data were fitted to equation 18 using a three parameter fit.

In $T_{1\rho}$ measurements, a single spin lock pulse was used, consisting of an adiabatic half passage to tilt the magnetization, a constant RF spin lock part (10-70 ms, three spin lock times) and another half passage to return the magnetization back to z-axis. The signal was detected similar to T_1 with TR of 3 s. Five B_1 fields were used, ranging from 0.2 G to 1.6 G, corresponding to frequency range of 0.86 - 6.9 kHz.

Single echo T_2 and T_2* were measured from 10-mm (1.5 T) or 2-mm (4.7 T) slice profiles. At 4.7 T it was necessary to exclude noise from the perimeter of the tube in a manner similar to one used in T_1 and $T_{1\rho}$ experiments. TEs for spin echo ranged from 20 to 200 ms at 1.5 T and from 10 to 200 at 4.7 T. For deoxygenated blood at 4.7 T, the longest TEs were only 100 ms, due to the dramatic shortening of T_2. For the gradient echo, TEs were 10-80 ms at 1.5 T and 10-40 ms at 4.7 T. TR in measurements of transverse relaxation was 3 s at both fields

CPMG T_2 was measured using hard pulses. Spins were tipped along x and refocusing pulses were applied along y, alternating in sign. The voxel was chosen using outer volume saturation. At 1.5 T, the refocusing interval τ_{CPMG} varied from 2 to 20 ms, 10 values were used. In the clinical scanner, TR had to be adjusted to 10 s so as not to exceed the limit for specific absorption rate. At 4.7 T, τ_{CPMG}, ranging from 1 ms to 20 ms in 11 steps, and TR of 3 s were used. For each τ_{CPMG}, four TEs were measured and R_2 was determined using a linearized 2-parameter fit.

4.2.3 Data analysis

R_1 (**I**) as function of blood oxygen level (Y) was measured from samples of three different hematocrits. The rates were fitted linearly to 1-Y and these interpolated rates at fixed oxygenation states (0.0, 0.1, 0.2 …1.0) were fitted to hematocrit, still linearly. The extrapolation of these hematocrit fits gives relaxation rates in plasma (Hct=0) and in erythrocytes (Hct=1).

$R_{1\rho}$ data (**II**) as a function of angular frequency of the spin locking field (ω_0) was fitted to a simple Lorentzian lineshape (equation 10). The three free parameters in this fit were the baseline relaxation rate $R_{1\rho,0}$, rate at very high B_1, the dispersion amplitude B_{LOR} and the correlation time τ_c. The relaxation rate at B_1=0 was given as a sum of baseline and dispersion amplitude.

The transverse relaxation rates determined with a CPMG sequence (**III**) were first fitted to a Luz-Meiboom equation (Equation 16). This yields the baseline relaxation rate $R_{2,0}$, the rate at infinitely high refocusing rate, correlation time τ_{exch} and the susceptibility difference $\Delta\omega$. As the first step, these fits were performed separately for each data set (Y and Hct). Since no dependence of τ_{exch} on oxygenation was expected and none detected, the τ_{exch} was fixed to remain the same for all samples of given hematocrit. The fits were run again for all hematocrits.

The values of $\Delta\omega$ were plotted as a function of deoxygenation and from a linear fit, the intra- to extracellular susceptibility shifts were determined for oxygenated and deoxygenated blood. In order to calculate the terms needed for blood calibration (van Zijl et al., 1998), the values of $R_{2,0}$ were further analyzed to find out $R_{2,ery}$, the relaxation rates in intracellular space. To achieve this, equation

$$R_{2,0} = (1 - Hct)R_{2,plasma} + HctR_{2,ery} \qquad \textbf{Equation 22}$$

was used. $R_{2,0}$ at full oxygenation were fitted linearly as a function of hematocrit to obtain the value of $R_{2,dia} + R_{2,oxy}$ (the slope of this fit) and value of $R_{2,plasma}$ (intercept). All $R_{2,ery}$ data were pooled and fitted as a function of deoxygenation. This line gives the relaxation rate in deoxygenated cells (at 1-Y=1) and in oxygenated cells (1-Y=0). As this set of equations is overdetermined, these two fits were performed simultaneously and the weighted sum of least squares was minimized.

The relaxation rate data from single spin echo and gradient echo experiments (**IV**) was further fitted as a function of 1-Y. As predicted by the LM equation and previous reports, quadratic dependence was apparent and polynomials

$$\begin{aligned} R_2 &= A + B(1-Y) + C(1-Y)^2 \\ R_2^* &= A^* + B^*(1-Y) + C^*(1-Y)^2 \end{aligned} \qquad \textbf{Equation 23}$$

and

$$\begin{aligned} R_2 &= A + C(1-Y)^2 \\ R_2^* &= A^* + C^*(1-Y)^2 \end{aligned} \qquad \textbf{Equation 24}$$

were used.

4.3 NMR methods and data analysis in fMRI

The fMRI experiments were carried out in the same 1.5 T Philips system used for blood experiments, with a body coil transmit and 12.5 mm surface coil receive. Eight volunteers were studied. A flashing checkerboard was shown in three 2-minute periods, each followed by a rest period. Ten high-resolution absolute T_2 images (CPMG spin echo: τ_{CPMG} 25 ms, TR 1 s, in-plane resolution 1.0 x 1.4 mm^2, 2 mm slice) were acquired during each period.

The purpose of the image analysis was to separate R_2 activation arising purely from blood vessels. To achieve this, strong correlation ($P<0.01$) to a boxcar activation pattern was required, which can be expected of BOLD changes in blood. Further, only the T_2 values between 100 and 250 ms were included, in order to exclude voxels containing tissue (T_2 less than 100 ms) and CSF. These blood R_2s were further analyzed and the oxygen extraction ratio was calculated using the calibration data from blood CPMG measurements.

4.4 Simulations of the NMR signal *in vivo*

4.4.1 Flow simulations (I)

The simulation of the effect of alterations in blood R_1 on flow determination was based on the model by Kwong et al (Kwong et al., 1992). This is the simplest model taking blood relaxation into account. There are more sophisticated models available complementing Kwong's model, which include e.g. blood-tissue exchange (Zhou and van Zijl, 1999) but the effect of blood relaxation rate should not differ greatly from the original model.

In the model, the measured parenchymal relaxation rate is a result of relaxation in blood and tissue:

$$R_{1,mixed} = (1 - CBVr) * R_{1,tissue} + CBVr * R_{1,blood} \qquad \textbf{Equation 25}$$

in which CBVr is the relative blood volume. In the model, both blood and tissue relaxation rates must be known. The rates are normally considered constant but in present simulations, blood R_1 is varied in the range expected to cover the physiological alteration of blood oxygenation and hematocrit. Now the measured apparent R_1 is

$$R_{1,app} = R_{1,mixed} + \frac{CBF}{\lambda} \qquad \textbf{Equation 26}$$

where CBF is cerebral blood flow and λ is the tissue water content (0.9 ml/g). Values of $R_{1,app}$ were simulated using low (0.34) and high (0.50) hematocrit and venous (Y=0.60) and arterial (Y=1.00) oxygenation levels for two flow levels (0.5 and 1.5 ml/g/min). The variation in blood relaxation rate is reflected in $R_{1,app}$ and the flow determined using equation 26 becomes biased. In the simulations, the calculated flow was compared to the actual flow (the flow that would be detected correctly if the blood were venous blood of hematocrit 0.40).

It should be noted that the simulation is independent of the value used for tissue relaxation rate and also the field strength, except through the possibly field-dependent amplitude of BOLD- and hematocrit-induced changes in $R_{1,blood}$. On the contrary, the effect of true flow level is robust. In the case of slow flow, even minor changes in blood rate result in large errors in flow but at higher flow levels, these errors are less significant.

4.4.2 BOLD-fMRI simulations (IV)

Based on the data on transverse relaxation in blood, we simulated the signal in an fMRI experiment. Physiological changes typical to visual activation were assumed: blood volume increase from 0.047 to 0.059 (resulting in a 58 % increase in CBF) and a 5 % increase in oxygen consumption ($CMRO_2$). Using the intravascular BOLD model (van Zijl et al., 1998), in which the signal from a voxel is a sum of signal coming from vascular and tissue pools, the changes as a function of echo time and field strength (1.5 and 4.7 T) were studied. In addition to changes in transverse relaxation, the contribution from repetition time and flip angle (different degree of saturation in pools of different R_1) and flow-sensitive $R_{1,app}$ were included. It should be noted that this approach deals with intravascular changes only and neglects the extravascular BOLD effects, more than half of the total R_2* BOLD response (Boxerman et al., 1995; Hoogenraad et al., 2001; Song et al., 1996) but this is minor in R_2 BOLD (Ogawa and Lee, 1990).

The BOLD signal change was presented as a function of echo time TE for pure parenchyma (tissue and microvessels) and for parenchyma containing partial voluming from small veins (2%) and arteries (0.8%). The relative contributions from different types of microvessels (arterioles, capillaries and venules) were plotted separately. As a test of reliability, data from fMRI experiments by other groups (Gati et al., 1997; Hoogenraad et al., 2001) were reproduced as closely as possible.

5 RESULTS

5.1 T_1 and flow simulations (I)

There was a clear effect of oxygenation state and the concentration of hemoglobin on the longitudinal relaxation. R_1 showed a linear dependence on both blood hematocrit and oxygenation. The hematocrit was the determining factor, as the relaxation rate in plasma was only 0.46 1/s and more than double in cells on the physiologic range of oxygenation. This was attributed to net macromolecule content in blood, affecting the fractions of free, slowly relaxing and protein-influenced, rapidly relaxing water. The effect of deoxygenation in normal blood was rather small but still significant: the venous relaxation rate was almost 20 % higher than the arterial rate.

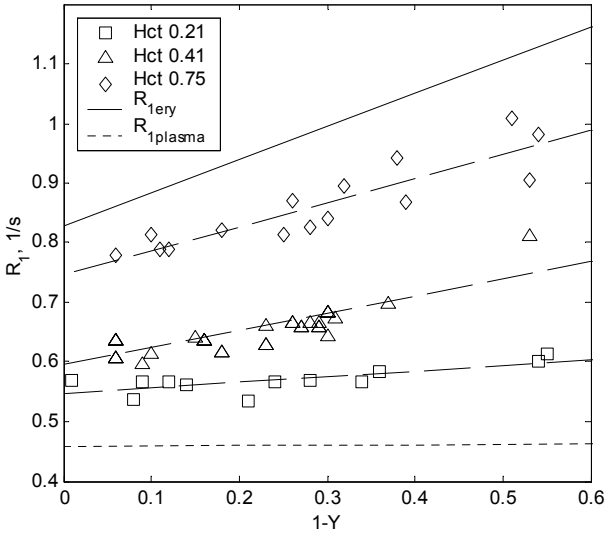

Figure 10: Measured R_1 relaxation rates in blood (dashed lines) and calculated rates in erythrocytes (solid line) and in plasma (dotted line), determined using equation 16. The dependence on oxygenation is the most evident in the samples of high hematocrit, but clearly visible also in physiological blood (triangles).

The effect of the variation in blood R_1 on determination of blood flow using ASL methods (Kwong model (Kwong et al., 1992)) was estimated by simulations. The influence on flow calculations was surprisingly large, especially at the lower flow level of 0.5 ml/g/min. The physiological alteration of hematocrit induced errors reaching 24 % in the most extreme case. If also the oxygen saturation was different from expected, the errors were further increased, up to 50 %. In the case of higher flow (150 ml/min/100g instead of 50 ml/min/100g), the errors were reduced to one third of the values for low flow.

The dissolved oxygen in plasma resulted in relaxation enhancement, with a magnitude similar to the BOLD-induced effects in blood of physiological hematocrit. The relaxation rate in the presence of excess O_2 was linearly dependent on the partial pressure of oxygen.

5.2 $T_{1\rho}$ and T_2 in blood and in lysate (II)

The blood relaxation in rotating frame showed in most cases an apparently linear dependence on both deoxygenation and hematocrit (Fig. 11 A-C). As the spin-lock field amplitude declined, the dependence on deoxygenation grew stronger and a tendency for deviation from linearity was seen. The pronounced effect of deoxygenation was evident also in dispersion amplitude (Fig. 12C) as the dispersion amplitude showed a strong, possibly quadratic response. The correlation times from single Lorentzian fits were around 40 μs for oxygenated blood and were lengthened by approx. 50 % as the blood was deoxygenated.

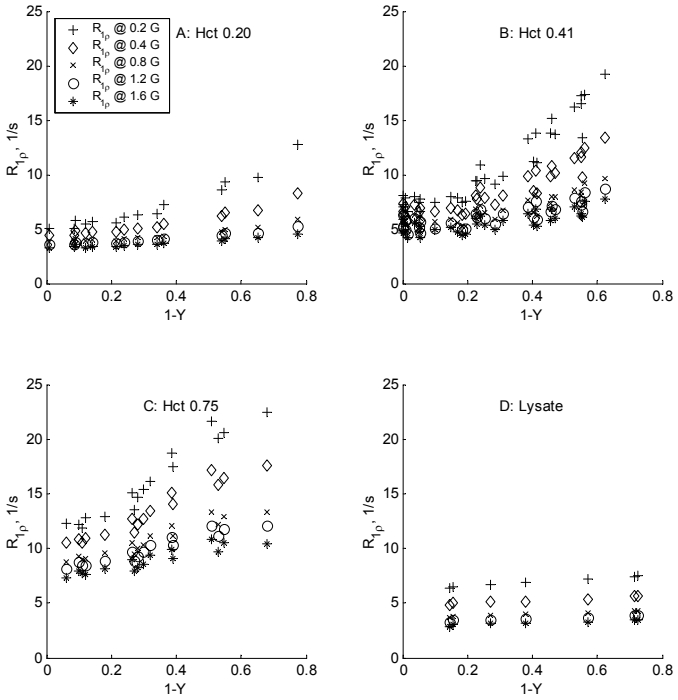

Figure 11: $R_{1\rho}$ is plotted as a function of deoxygenation, at several B_1 fields for blood of different hematocrits (A-C) and for blood lysate (D). The dispersion is much more pronounced in blood compared to lysate. In addition, the NMRD in blood shows a strong dependency on oxygenation, whereas in lysate that parameter is virtually independent of Y.

The importance of compartmentalization of Hb into erythrocytes was investigated by repeating the measurements in cell-free blood lysate. The relaxation in lysate differed from that in whole blood (Fig. 10 D). First, the oxygenation dependence in lysate was not as prominent as in blood. Second, the dispersion data provided correlation times comparable to blood, though now without any dependence on oxygenation. The deoxygenation increased only the baseline of the dispersion curve, whereas in blood also the dispersion amplitude was strongly dependent on oxygenation. Two possible reasons for this were given: the motional state of Hb in intracellular space is different from that in lysate and this may have been reflected in the relaxation and, as a second factor, the difference in Larmor frequencies at cell membrane may impair the spin lock and the contribution of those spins to measurement relaxation rate is no more determined by $R_{1\rho}$.

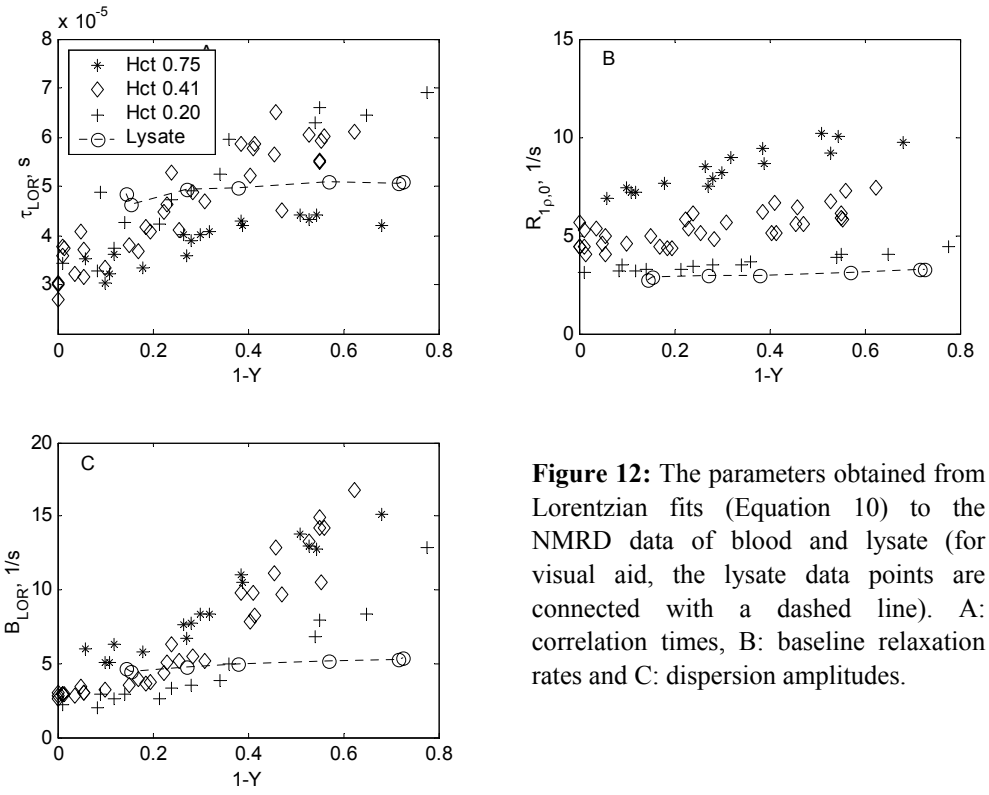

Figure 12: The parameters obtained from Lorentzian fits (Equation 10) to the NMRD data of blood and lysate (for visual aid, the lysate data points are connected with a dashed line). A: correlation times, B: baseline relaxation rates and C: dispersion amplitudes.

The transverse single echo relaxation rate further demonstrated the difference between the cell-free lysate and whole blood. In the oxygenated state, the relaxation rate in blood of normal hematocrit was approximately 50 % higher than that in lysate, containing same amount of Hb. As the preparations were deoxygenated by 50 %, the R_2 in lysate was elevated marginally but increased to 5-6 fold in blood. Furthermore, the dependence on deoxygenation was linear in lysate but quadratic in blood. This behavior could be expected, as the dephasing-related relaxation processes in whole blood are known to originate from erythrocytes, rather than Hb molecules directly, and follow quadratically the degree of deoxygenation.

5.3 T_2 measurements using CPMG in blood and in humans (III)

The CPMG data from 1.5 T shows that the Luz-Meiboom equation (Equation 21) describes blood relaxation in a wide range of hematocrits and blood oxygenation levels. The mean correlation time determined from these fits was 2.5 ms, independent of hematocrit. The susceptibility shift was 0.31 ppm between oxygenated and deoxygenated blood, and the residual susceptibility shift from plasma to oxygenated cells was 0.06 ppm, indicative of a shift of 0.39 ppm between plasma and fully deoxygenated cells. The analysis of baseline ($t_{CPMG} \rightarrow 0$) rrelaxation rates provides values of 1.6 1/s for plasma and 5.5 1/s + 8.1 1/s*(1-Y) for erythrocytes. The calibration parameters were determined also in human blood and no significant difference from bovine blood was found (Silvennoinen et al., 2001).

A similar set of CPMG measurements at 4.7 T resulted in a correlation time of 1.2±0.3 ms (mean of all hematocrits ± standard deviation). In this data, the highest hematocrit (0.75) was deviant; if that correlation time (0.8 ms) was excluded, the average correlation time from other hematocrits (0.21, 0.41 and 0.57) was 1.29±0.08 ms. At 9.4 T (Silvennoinen et al., 1999), the determined correlation in bovine blood time was 1.1 ms. Susceptibility shifts between plasma and deoxygenated cells, determined at 4.7 and 9.4 T, were 0.47 ppm (Hct 0.41) and 0.37 ppm respectively.

The CPMG data from 1.5 T was applied in the determination of the oxygen extraction ratio in humans *in vivo*. The analysis of activation in small vessels in visual cortex yielded OER values of 0.38±0.04 for baseline activity and 0.18±0.06 (mean ± standard deviation) for the activated state. The results are well in line with values reported in experiments using either positron emission tomography (Fox et al., 1988; Leenders et al., 1990; Marchal et al., 1992) or MRI (Haacke et al., 1997; Oja et al., 1999). In comparison to use of the single spin echo R_2s, the CPMG method has several advantages. First, the values of blood R_2s are lower using CPMG, increasing the contribution from blood pool and overall signal-to-noise ratio. Secondly, as the relaxation in tissue is less sensitive to the choice of sequence than the situation in blood, the contrast between blood and tissue is better in CPMG images than in single echo data.

5.4 Comparison between T_2 and T_2* (IV)

In this part, BOLD-dependence of single echo R_2 and R_2* at 1.5 T and 4.7 T were fitted using a quadratic function. In all cases, a polynomial with zeroth and second term was satisfactory. The main result is that there is no additional BOLD-dependent term in R_2* but the gradient echo relaxation in isolated blood can be expressed through spin echo relaxation plus a constant, facilitating the modeling of intravascular R_2*. The value of this constant naturally depends on the experimental parameters, especially the field homogeneity, and, at least to some degree, on hematocrit. The gradient echo profiles at 4.7 T were remarkably worse than spin echo profiles (Figure 13 A, C, E and G), and the same was evident when R_2* and R_2 profiles were compared (Figure 13 B, D, F and H). This suggests that at high fields, R_2 is a more reliable parameter *in vivo* than R_2*, at least in quantitative applications of MRI.

The simulations of intravascular fMRI signal at 1.5 and 4.7 T revealed some interesting points. First, the dependence on echo time was different at 1.5 T and 4.7 T. At 1.5 T the relative BOLD change increased steadily with TE while at 4.7 T there was a plateau followed by a decrease in the BOLD change. Second, the contribution from different vascular pools varied according to the field. At low field, the contributions followed the volume of the compartments with the largest venous compartment predominating. At 4.7 T, however, the high R_2 of venous blood attenuated that compartment and the capillary signal predominated. At long TEs, even the arterial pool became significant. This also resulted in perhaps unexpectedly small BOLD at 4.7 T. However, the extravascular BOLD effect in a gradient echo experiment will not experience any such attenuation induced by high relaxation rates.

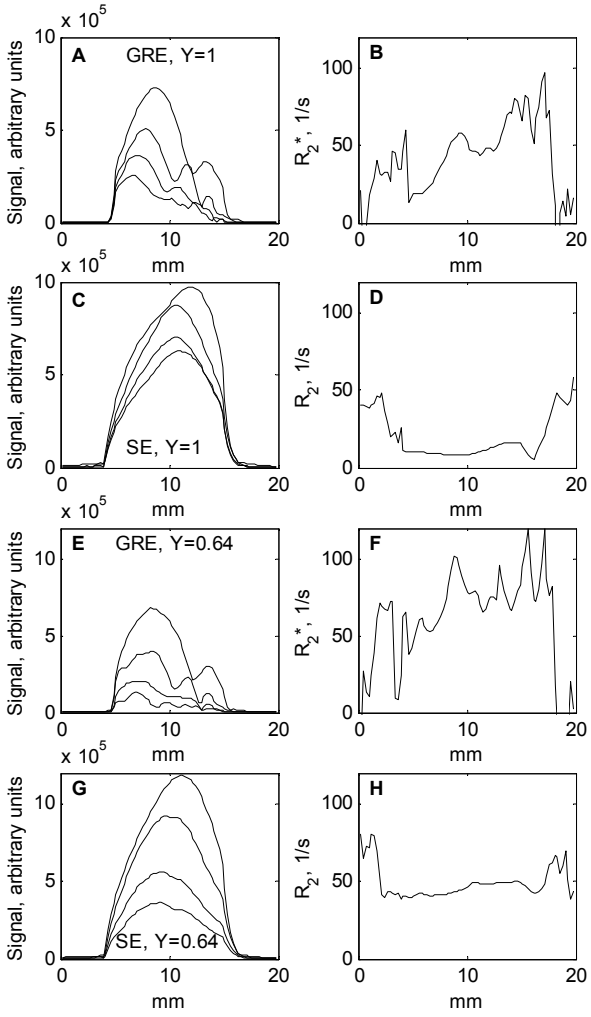

Figure 13: Measurements of a blood phantom at 4.7 T. Signal intensities at different TEs (A, C, E and G) and corresponding relaxation rate profiles (B, D, F and H). The distortion of the profile of gradient echo data is seen in both the signal and R_2.

6 DISCUSSION

The present work characterizes the main relaxation parameters and their dependence on the physiological state of blood. Relaxation in blood is a sum of several mechanisms. In R_1, direct effects of the hemoglobin concentration (hematocrit) and the degree of paramagnetism (oxygenation) are seen, both resulting in linear dependencies. This provides a baseline upon which other mechanisms are added. The effects of the susceptibility shift between intra- and extracellular spaces are detected in transverse relaxation and, to some degree, in low spin lock field $R_{1\rho}$. The measurement of a gradient echo instead of a spin echo does not seem to provide any additional oxygenation-dependent mechanisms, but rather a constant increase in relaxation rate.

6.1 Longitudinal relaxation

The fact that blood R_1 shows dependence on oxygenation may seem unexpected, as it has been claimed that the paramagnetic center in a Hb molecule is unapproachable to water and thus there should not be any influence of deoxygenation on R_1 (Brooks and Di Chiro, 1987; Gomori et al., 1987; Matwiyoff et al., 1991) or at least it should remain very small (Bryant et al., 1990). Indeed, the effect in R_1 is small compared to BOLD seen in R_2 and this difference may reflect indirect transfer of magnetization within the Hb molecule through cross-relaxation processes, instead of direct coupling between water and the iron. This view is supported by the observation of a single R_1 in Hb, resulting from fast intramolecular relaxation (Eisenstadt and Fabry, 1978). In contrast to oxygenation, the dependence of R_1 on hematocrit was anticipated as it has been demonstrated earlier (Bryant et al., 1990). The protein content has been shown to influence R_1 in immobile protein solutions (Jiao and Bryant, 1996) and in blood, the net macromolecule content depends linearly on hematocrit.

The determined values for R_1 agree well with those reported earlier (Bryant et al., 1990), even if higher rates have been proposed in some studies as well. There are several possible reasons for the variation in literature R_1, as both blood itself (oxygenation, hematocrit), blood handling (clotting, precipitation) and experimental conditions (temperature, the method of the measurement) can influence on the result.

The NMRD profiles from spin-lock experiments fit well to a single Lorentzian line shape, suggesting that the system is well characterized by a single apparent correlation time. As the range of B_1 in the study is rather narrow, the measured correlation time is by no means the only one present in the system. Furthermore, even within this range there may be several correlation times contributing to the measured apparent correlation time. On the other hand, the closeness of zero-field $R_{1\rho}$ to baseline transverse relaxation rate does not leave space for any dramatic twists in the dispersion curve at low frequencies. Specifying the exact mechanism accounting for the NMRD behavior is not possible from the data presented in this work. However, since it was observed during the experiments that $R_{1\rho}$ at full oxygenation is quite sensitive to alterations

in pH, some role of proton exchange may be considered, since the effect of pH on water exchange and membrane permeability (Morariu et al., 1981) is small.

The water transport through the erythrocyte membrane may play some role in low-B_1 dispersion. Especially at low oxygenation, the dispersion profile is distinctly steeper than that seen in lysate. In **II**, the sudden jump across the membrane was proposed to drop the spins out of spin-lock and enable transverse relaxation to take place. The time of crossing required for this was estimated based on the abrupt shift in resonance frequencies, resulting in a very probable loss of spin-lock. However, the field variation is not so steep in reality and, furthermore, behaves differently depending on the location on the cell surface as well as on the orientation relative to the main field (Gillis et al., 1995). Nonetheless, it is plausible that the spin-lock conditions are compromised and that can be seen in dispersion at low B_1 and low oxygen saturation. In addition, the absence of dispersion in packed erythrocytes (Zipp et al., 1977) points to a role for cross-membrane exchange. Another possible effect would be a dramatic change in mobility and/or structure of Hb between lysate and cells. However, it has been shown that the restriction in mobility in cells is rather small (Blinc et al., 1990; Lindstrom et al., 1976; Wang et al., 1997) and, since the blood samples and lysate are prepared from the same blood, differences in structure are not likely.

6.2 Transverse relaxation

The calibration values from blood CPMG measurements were tested *in vivo* in the determination of OER during baseline activity and visual stimulation. The results are in good agreement with literature data on cerebral OER changes (An and Lin, 2000; Cohen et al., 1967; Fox et al., 1988; Haacke et al., 1997; Leenders et al., 1990; Marchal et al., 1992; Oja et al., 1999) considering the differences in measurement methods and stimulation paradigms.

The calibration provides, as a side-product, correlation times from the Luz-Meiboom fits. Originally, the equation was for two-site exchange and the cross-membrane exchange could possibly be treated as such. The correlation times for this exchange are expressed by Equation 1, for normal hematocrit a value of 7 ms would be expected and that should be shortened as the hematocrit is increased. At 4.7 T, the correlation time was 1.3 ms and at 9.4 T, 1.1 ms, both values being independent of hematocrit. The times are well in line with previous reports (Gillis et al., 1995; Gomori et al., 1987; Meyer et al., 1995; Thulborn et al., 1982). In addition, at 9.4 T rat blood was used. In rodents, the erythrocyte membrane is more permeable to water than in large mammals (Benga and Borza, 1995), resulting in shorter exchange times. Another experiment was performed on pCMBS-treated bovine blood, where the water transport was shown to be reduced by 50 % by blocking the aquaporin-1 water channels (Benga and Borza, 1995). In both cases, the correlation times did not change significantly, despite the alteration in permeability. As in the cases of very deoxygenated blood and low hematocrit, the system approaches the intermediate region (exchange time is approximately 10 ms and susceptibility shift 0.4 ppm), also the equations for intermediate exchange (Davis et al., 1994) were tested. The results were nearly identical to LM, as it would be expected according to the paper on the flexibility of fast exchange criteria of Allerhand and Gutowsky (Allerhand and Gutowsky, 1964).

This behavior of the correlation times argues against a role for cross-membrane exchange. On the other hand, both the hematocrit-independence, insensitivity to permeability and shortening as B_0 increases, fit well to diffusion-based dephasing. One would intuitively expect slower dephasing as the hematocrit reaches the point where field gradients from neighboring cells start to overlap and the pure plasma regions disappear, decreasing the amplitude of field gradients.

The determined susceptibility shifts (in ppm units) at high fields are comparable to the 1.5 T data. They also correspond well to literature data, both from CPMG-experiments (Gillis et al., 1995; Meyer et al., 1995; Thulborn et al., 1982) and from other methods (Alpert and Banerjee, 1975; Cerdonio et al., 1978; Spees et al., 2001; Weisskoff and Kiihne, 1992).

When gradient echoes are used instead of long-TE single spin echoes, the transverse relaxation increases by a term that depends on the shim, the main field and the hematocrit. However, this term seems to be independent of BOLD, suggesting that the amplitude of field gradients is not significant in the difference rate R_2' (= R_2*- R_2). This is expected, as in the long-TE single spin echo experiments the time constant of the dephasing by erythrocytes and Hb (a few milliseconds) is short compared to the echo times (10 ms or longer), resulting in nearly complete dephasing between the echoes and very inefficient refocusing. The absence of refocusing pulses in gradient echo experiments does not make the situation any worse and the R_2 effects dominate the BOLD.

When considering R_2 and R_2* *in vivo*, an additional factor in R_2* from tissue-vessel susceptibility shift is to be expected (Hoogenraad et al., 2001). However, in the light of the *in vitro* and *in vivo* data presented by Li et al. (Li et al., 1998), this does not seem to be a major contributor, as the relaxation rates determined *in vivo* and *in vitro* are equal within the error.

6.3 Simulations of flow and fMRI experiments

The simulations of blood flow experiments using the Kwong model (Kwong et al., 1992) show that the effect of blood R_1 on flow determination is very significant. The use of erroneous values for blood relaxation may lead to severe bias in assessment of the flow, especially in the case of low flow values and high blood volume, for instance from partial voluming from a vessel. The examples simulated in **I** are extreme cases, but the bias e.g. from the variation in hematocrit due to gender differences may be a source of significant error.

The simulations of the fMRI signal reveal some interesting aspects on the importance of intravascular BOLD and its relation to field strength. The BOLD in blood naturally increases with the field. However, the main issue for the behavior of parenchymal signal is the balance between relaxation rates in different types of blood (arterial, venous) and tissue. At low field (1.5 T and lower), blood R_2 is always lower than the corresponding value in tissue and the BOLD is largest at long TEs, although the contrast-to-noise ratio naturally decreases at very long TE. If blood R_2 is lower than that of tissue, an increase in CBV induces a decrease in voxel R_2 and this naturally increases the signal. It has been shown in several studies (Frahm et al., 1994; Oja et al., 1999) that the low field BOLD originates mainly from venules and small veins. At 4.7 T, venous R_2 is equal or higher than R_2 in tissue. This reduces the contribution from the

venous compartment in the net signal. In addition, the effect of CBV increase in venous region becomes less significant, or even negative, as the difference in R_2 between the tissue and vessel pools is small. As TE is increased, the weight of the venous compartment decreases and capillaries and even arteries start to dominate the observed BOLD. It should be noted that in arteries there is no real BOLD, as the arterial oxygenation remains the same, but the observed signal change is due to CBV changes. In practice, as the blood R_2 is very sensitive to the choise of the spin echo sequence, the signal loss due to blood relaxation at high field can be partially compensated by using short-τ CPMG instead of single spin echoes.

The above effects together diminish the fMRI signal change at high fields, but on the other hand, the source of the signal is moved towards the capillary region and thus closer to the activation site. In R_2*, the behavior inside the vessels is similar to R_2, but the extravascular effects are not attenuated in the high field. As the changes in blood R_2* are largest in the venous compartment, the net R_2* fMRI signal changes in the high field do not localize to the capillaries as R_2 changes.

6.4 Implications

The study propounds new concrete arguments to the ongoing discussion on field dependence and magnitude and localization BOLD. The current opinion of capillary-dominated BOLD at high field strengths (Lee et al., 1999; Ugurbil et al., 1999) is supported by the data, but the intravascular effects are, perhaps surprisingly, small due to the reduced blood relaxation times at high field. In addition, the contribution from CBV changes at high field is small (in the cases when blood $R_2 \approx$ tissue R_2) or even negative (blood $R_2 >$ tissue R_2, which is the case with low oxygen saturation at 4.7 T and with all venous blood at 9.4 T). The use of gradient echoes would solve the problem, as the extravascular field gradients are independent of the relaxation rate of blood. However, the comparison of high-field spin echo and gradient echo profiles (**III**) does not favor the use of gradient echoes, at least in applications using quantitative information of image intensity or relaxation rates.

One interesting solution to BOLD attenuation due to high blood relaxation rates might be the use of $R_{1\rho}$. As the longitudinal relaxation in blood is less sensitive to susceptibility than transverse processes, blood $R_{1\rho}$ remains lower than the corresponding value in tissue at 4.7 T and presumably that is the case also at higher field strengths. The more modest oxygenation effect in $R_{1\rho}$ could be compensated for by the larger contribution from blood volume changes. In the light of the present results, the most suitable spin lock field should be small, less than 1 G, as in that region the dependence of $R_{1\rho}$ on oxygenation is steepest. The use of low B_1 fields helps also in keeping the specific absorption rates (SARs) below the limits, a common practical problem in *in vivo* spin lock applications.

7 SUMMARY AND CONCLUSIONS

Longitudinal (R_1, $R_{1\rho}$) and transverse (R_2 and R_2*) relaxation in blood was studied at body temperature as a function of blood oxygen saturation and hematocrit at 1.5 and 4.7 T. The main findings in this work and their relevance to *in* vivo experiments can be summarized as follows

1) Blood oxygen saturation level affects all relaxation rates (R_1, $R_{1\rho}$, CPMG-R_2 and single echo R_2 and R_2*). The effect is rather small but still significant in R_1 and maximal in single echo R_2. In longitudinal relaxation, the effect was attributed to interaction between water and hemoglobin molecules whereas in transverse relaxation the additional dephasing effects, due to susceptibility inhomogeneities, predominate.

2) Blood hematocrit influences the relaxation rates. In comparison to BOLD, hematocrit dependence is more important in longitudinal relaxation and minor in transverse relaxation. The hematocrit-related effects are present *in vivo*, as the hematocrit may vary between healthy individuals and vessel types by 10 % to 20 %.

3) These effects, especially BOLD, in transverse relaxation are well known and usually accounted for, and in many cases even exploited, in models of hemodynamics. In this work, the determination of R_2 was used in quantification of oxygen extraction rates upon visual activation and intravascular signal changes in fMRI experiments were simulated. However, also the oxygenation- and hematocrit-related effects in longitudinal relaxation, albeit being less dramatic than in the transverse case, may produce significant bias in quantification.

8 REFERENCES

Allerhand, A., and Gutowsky, H. S. (1964). Spin-echo NMR studies of chemical exchange. I. Some general aspects. J Chem Phys *41*, 2115-2126.

Alpert, Y., and Banerjee, R. (1975). Magnetic susceptibility measurements of deoxygenated hemoglobins and isolated chains. Biochim Biophys Acta *405*, 144-154.

An, H., and Lin, W. (2000). Quantitative measurements of cerebral blood oxygen saturation using magnetic resonance imaging. J Cereb Blood Flow Metab *20*, 1225-1236.

Andrasko, J. (1976). Water diffusion permeability of human erythrocytes studied by a pulsed gradient NMR technique. Biochim. Biophys. Acta *428*, 304-311.

Andrasko, J. (1975). Water in agorose gels studied by nuclear magnetic resonance relaxation in the rotating frame. Biophys J *15*, 1235-1243.

Atalay, M. K., Reeder, S. B., Zerhouni, E. A., and Forder, J. R. (1995). Blood oxygenation dependence of T_1 and T_2 in the isolated, perfused rabbit heart at 4.7 T. Magn Reson Med *34*, 623-627.

Bandettini, P. A., Wong, E. C., Hinks, R. S., Tikofsky, R. S., and Hyde, J. S. (1992). Time course EPI of human brain function during task activation. Magn Reson Med *25*, 390-397.

Barth, M., and Moser, E. (1997). Proton NMR relaxation times of human blood samples at 1.5 T and implications for functional MRI. Cell Mol Biol (Noisy-le-grand) *43*, 783-791.

Benga, G. (1989). Water exchange through the erythrocyte membrane. Int Rev Cytol *114*, 273-316.

Benga, G., and Borza, T. (1995). Diffusional water permeability of mammalian red blood cells. Comp Biochem Physiol B Biochem Mol Biol *112*, 653-659.

Blinc, A., Lahajnar, G., Blinc, R., Zidansek, A., and Sepe, A. (1990). Proton NMR study of the state of water in fibrin gels, plasma, and blood clots. Magn Reson Med *14*, 105-122.

Bottomley, P. A., Foster, T. H., Argersinger, R. E., and Pfeifer, L. M. (1984). A review of normal tissue hydrogen NMR relaxation times and relaxation mechanisms from 1-100 MHz: dependence on tissue type, NMR frequency, temperature, species, excision, and age. Med Phys *11*, 425-448.

Boxerman, J. L., Hamberg, L. M., Rosen, B. R., and Weisskoff, R. M. (1995). MR contrast due to intravascular magnetic susceptibility perturbations. Magn Reson Med *34*, 555-566.

Brindle, K. M., Brown, F. F., Cambell, I. D., Grathwohl, C., and Kuchel, P. W. (1979). Application of spin-echo nuclear magnetic resonance to whole-cell systems. Biochem. J. *180*, 37-44.

Brix, G., Schad, L. R., Deimling, M., and Lorenz, W. J. (1990). Fast and precise T_1 imaging using a TOMROP sequence. Magn Reson Imaging *8*, 351-356.

Brooks, R. A. (2002). T_2-shortening by strongly magnetized spheres: a chemical exchange model. Magn Reson Med *47*, 388-391.

Brooks, R. A., Battocletti, J. H. S., Sances, A. J., Larson, S. J., Bowman, R. L., and Kudravcev, V. (1975). Nuclear magnetic relaxation in blood. IEEE T Bio-Med Eng *BME-22*, 12-18.

Brooks, R. A., Brunetti, A., Alger, J. R., and Di Chiro, G. (1989). On the origin of paramagnetic inhomogeneity effects in blood. Magn Reson Med *12*, 241-248.

Brooks, R. A., and Di Chiro, G. (1987). Magnetic resonance imaging of stationary blood: a review. Med Phys *14*, 903-913.

Brooks, R. A., Moiny, F., and Gillis, P. (2001). On T_2-shortening by weakly magnetized particles: the chemical exchange model. Magn Reson Med *45*, 1014-1020.

Brooks, R. A., Vymazal, J., Bulte, J. W., Baumgarner, C. D., and Tran, V. (1995). Comparison of T_2 relaxation in blood, brain, and ferritin. J Magn Reson Imaging *5*, 446-450.

Brown, F. F. (1983). The effects of compartmental location on the proton T_2* of small molecules in cell suspensions: A cellular field gradient model. J Magn Reson *54*, 385-399.

Brown, R. J. S. (1961). Distribution of fields from randomly placed dipoles: free-precession signal decay as result of magnetic grains. Phys Rev *121*, 1379-1382.

Bryant, R. G. (1996). The dynamics of water-protein interactions. Annu Rev Biophys Biomol Struct *25*, 29-53.

Bryant, R. G., Marill, K., Blackmore, C., and Francis, C. (1990). Magnetic relaxation in blood and blood clots. Magn. Reson. Med. *13*, 133-144.

Calamante, F., Thomas, D. L., Pell, G. S., Wiersma, J., and Turner, R. (1999). Measuring cerebral blood flow using magnetic resonance imaging techniques. J Cereb Blood Flow Metab *19*, 701-735.

Cameron, I. L., Ord, V. A., and Fullerton, G. D. (1988). Water of hydration in the intra- and extra-cellular environment of human erythrocytes. Biochem Cell Biol *66*, 1186-1199.

Cerdonio, M., A., C.-C., Calabrese, L., Morante, S., Pispisa, B., and Vitale, S. (1978). Room.temperature magnetic properties of oxy- and carbonmonoxyhemoglobin. Proc. Natl. Acad. Sci. *75*, 4916-4919.

Chien, D., Levin, D. L., and Anderson, C. M. (1994). MR gradient echo imaging of intravascular blood oxygenation: T_2* determination in the presence of flow. Magn Reson Med *32*, 540-545.

Chopra, S., McClung, R. E. D., and Jorda, R. B. (1984). Rotating-frame relaxation rates of solvent molecules in solutions of paramagnetic ions undergoing solvent exchange. J Magn Reson *59*, 361-372.

Cohen, P. J., Alexander, S. C., Smith, T. C., Reivich, M., and Wollman, H. (1967). Effects of hypoxia and normocarbia on cerebral blood flow and metabolism in conscious man. J Appl Physiol *23*, 183-9.

Cottam, G. L., and Waterman, M. R. (1976). Effect of oxygen concentration on trasverse water proton relaxation times in erythrocytes homozygous and heterozygous for hemoglonin S. Arch Biochem Biophys *177*, 293-298.

Cowan, B. P. (1997). Nuclear Magnetic Resonance and Relaxation, First Edition (Cambridge: Cambridge University Press).

Darquie, A., Poline, J. B., Poupon, C., Saint-Jalmes, H., and Le Bihan, D. (2001). Transient decrease in water diffusion observed in human occipital cortex during visual stimulation. Proc Natl Acad Sci U S A *98*, 9391-9395.

Davis, D. G., Perlman, M. E., and London, R. E. (1994). Direct measurements of the dissociation-rate constant for inhibitor-enzyme complexes via the $T_{1\rho}$ and T_2 (CPMG) methods. J Magn Reson B *104*, 266-275.

de Certaines, J. D., Bovee, W. M. M. J., and Podo, F. (1992). Magnetic resonance spectroscopy in biology and medicine: Pergamon Press Ltd.).

Detre, J. A., and Alsop, D. C. (1999). Perfusion magnetic resonance imaging with continuous arterial spin labeling: methods and clinical applications in the central nervous system. Eur J Radiol *30*, 115-124.

Duvvuri, U., Goldberg, A. D., Kranz, J. K., Hoang, L., Reddy, R., Wehrli, F. W., Wand, A. J., Englander, S. W., and Leigh, J. S. (2001). Water magnetic relaxation dispersion in biological systems: the

contribution of proton exchange and implications for the noninvasive detection of cartilage degradation. Proc Natl Acad Sci U S A *98*, 12479-12484.

Eisenstadt, M. (1985). NMR relaxation of protein and water protons in diamagnetic hemoglobin solutions. Biochemistry *24*, 3407-3421.

Eisenstadt, M., and Fabry, M. E. (1978). NMR relaxation of the hemoglobin-water proton spin system in red blood cells. J Magn Reson *29*, 591-597.

Engelhardt, R. T., and Johnson, G. A. (1996). $T_{1\rho}$ relaxation and its application to MR histology. Magn. Reson. Med. *35*, 781-786.

Fabry, M. E., and San George, R. C. (1983). Effect of magnetic susceptibility on nuclear magnetic resonance signals arising from red cells. Biochemistry *22*, 4119-4125.

Ferrari, M., Wilson, D. A., Hanley, D. F., and Traystman, R. J. (1992). Effects of graded hypotension on cerebral blood flow, blood volume, and mean transit time in dogs. Am J Physiol *262*, H1908-H1914.

Fox, P. T., Raichle, M. E., Mintun, M. A., and Dence, C. (1988). Nonoxidative glucose consumption during focal physiologic neural activity. Science *241*, 462-464.

Frahm, J., Merboldt, K. D., Hanicke, W., Kleinschmidt, A., and Boecker, H. (1994). Brain or vein--oxygenation or flow? On signal physiology in functional MRI of human brain activation. NMR Biomed *7*, 45-53.

Fujita, N. (2001). Extravascular contribution of blood oxygenation level-dependent signal changes: a numerical analysis based on a vascular network model. Magn Reson Med *46*, 723-34.

Gasparovic, C., and Matwiyoff, N. A. (1992). The magnetic properties and water dynamics of the red blood cell: a study by proton-NMR lineshape analysis. Magn Reson Med *26*, 274-299.

Gati, J. S., Menon, R. S., Ugurbil, K., and Rutt, B. K. (1997). Experimental determination of the BOLD field strength dependence in vessels and tissue. Magn Reson Med *38*, 296-302.

Gillis, P., and Koenig, S. H. (1987). Transverse relaxation of solvent protons induced by magnetized spheres: application to ferritin, erythrocytes, and magnetite. Magn Reson Med *5*, 323-345.

Gillis, P., Moiny, F., and Brooks, R. A. (2002). On T_2-shortening by strongly magnetized spheres: a partial refocusing model. Magn Reson Med *47*, 257-263.

Gillis, P., Peto, S., Moiny, F., Mispelter, J., and Cuenod, C. A. (1995). Proton transverse nuclear magnetic relaxation in oxidized blood: a numerical approach. Magn Reson Med *33*, 93-100.

Gillis, P., Roch, A., and Brooks, R. A. (1999). Corrected equations for susceptibility-induced T_1-shortening. J Magn Reson *137*, 402-407.

Gomori, J. M., Grossman, R. I., Yo-Ip, C., and Asakura, T. (1987). NMR relaxation times of blood: dependence on field strength, oxidation state, and cell integrity. J. Comput. Assist. Tomo. *11*, 684-690.

Grubb, R. L., Jr., Raichle, M. E., Eichling, J. O., and Ter-Pogossian, M. M. (1974). The effects of changes in P_aCO_2 on cerebral blood volume, blood flow, and vascular mean transit time. Stroke *5*, 630-639.

Gueron, M. (1975). Nuclear relaxation in macromolecules by paramagnetic ions: a novel mechanism. J Magn Reson *19*, 58-66.

Guyton, A. C. (1986). Textbook of Medical Physiology, Seventh Edition, D. D., ed.: W. B. Saunders Company).

Haacke, E. M., Lai, S., Reichenbach, J. R., Kuppusamy, K., Hoogenraad, F. G. C., Tackeichi, H., and Lin, W. (1997). In vivo measurement of blood oxygen saturation using magnetic resonance imaging: a direct

validitation of the blood oxygen level-dependent concept in functional brain imaging. Hum Brain Map *5*, 341-346.

Hallenga, K., and Koenig, S. H. (1976). Protein rotational relaxation as studied by solvent ^{1}H and ^{2}H magnetic relaxation. Biochemistry *15*, 4255-4264.

Hardy, P., and Henkelman, R. M. (1991). On the transverse relaxation rate enhancement induced by diffusion of spins through inhomogeneous fields. Magn Reson Med *17*, 348-356.

Hayman, L. A., Ford, J. J., Taber, K. H., Saleem, A., Round, M. E., and Bryan, R. N. (1988). T_2 effect of hemoglobin concentration: assessment with in vitro MR spectroscopy. Radiology *168*, 489-491.

Henkelman, R. M., Neil, J. J., and Xiang, Q. S. (1994). A quantitative interpretation of IVIM measurements of vascular perfusion in the rat brain. Magn Reson Med *32*, 464-9.

Heymann, J. B., Agre, P., and Engel, A. (1998). Progress on the structure and function of aquaporin 1. J Struct Biol *121*, 191-206.

Hoffman, R., Benz Jr, E. J., Shattil, S. J., Furie, B., Cohen, H. J., Silberstein, L. E., and McGlave, P. (2000). Hematology - Basic Principles and Practice, 3rd Edition (New York NY: Churchill Livingstone).

Hoogenraad, F. G., Pouwels, P. J., Hofman, M. B., Reichenbach, J. R., Sprenger, M., and Haacke, E. M. (2001). Quantitative differentiation between BOLD models in fMRI. Magn Reson Med *45*, 233-246.

Intaglietta, M., Johnson, P. C., and Winslow, R. M. (1996). Microvascular and tissue oxygen distribution. Cardiovasc Res *32*, 632-643.

Ishima, R., and Torchia, D. A. (1999). Estimating the time scale of chemical exchange of proteins from measurements of transverse relaxation rates in solution. J Biomol NMR *14*, 369-372.

Jen, J. (1978). Chemical exchange and NMR T_2 relaxation - The multisite case. J Magn Reson *30*, 111-128.

Jensen, J. H., and Chandra, R. (2000). NMR relaxation in tissues with weak magnetic inhomogeneities. Magn Reson Med *44*, 144-156.

Jiao, X., and Bryant, R. G. (1996). Noninvasive measurement of protein concentration. Magn. Reson. Med. *35*, 159-161.

Kaplan, J. I. (1980). NMR line shape in the region where the chamical exchange time t_e approaches the motional exchange time t_c. Phys Rev A *22*, 1022-1024.

Kennan, R. P., Zhong, J., and Gore, J. C. (1994). Intravascular susceptibility contrast mechanisms in tissues. Magn Reson Med *31*, 9-21.

Kiselev, V. G., and Posse, S. (1999). Analytical model of susceptibility-induced MR signal dephasing: effect of diffusion in a microvascular network. Magn Reson Med *41*, 499-509.

Kiselev, V. G., and Posse, S. (1998). Analytical theory of susceptibility induced NMR signal dephasing in cerebral network. Phys Rev Lett *81*, 5696-5699.

Knispel, R. R., and Pintar, M. M. (1975). Tempreature dependence of proton exchange time in pure water by NMR. Chem Phys Lett *32*, 238-240.

Knispel, R. R., Thompson, R. T., and Pintar, M. M. (1974). Dispersion of Proton Spin-Lattice Relaxation in Tissues. J Magn. Res. *14*, 44-51.

Koenig, S. H. (1999). Dynamics of water in biological systems: inferences from relaxometry. In Encyclopedia of Nuclear Magnetic Resonance, D. M. Grant and R. K. Harris, eds. (New York: John Wiley & Sons Ltd), pp. 1819-1830.

Koenig, S. H., and Brown III, R. D. (1994). Relaxometry and the source of contrast in MRI. In NMR in physiology and biomedicine, R. J. Gillies, ed. (San Diego, USA: Academic Press), pp. 57-73.

Koenig, S. H., Brown III, R. D., and Ugolini, R. (1993). A unified view of relaxation in protein solutions and tissue, including hydration and magnetization transfer. Magn Reson Med *29*, 77-83.

Koenig, S. H., and Brown, R. D., 3rd (1984). Determinants of proton relaxation rates in tissue. Magn Reson Med *1*, 437-449.

Koenig, S. H., Brown, R. D. I., and Ugolini, R. (1993). Magnetization transfer in cross-linked bovine serum albumin solutions at 200 MHz: A model for tissue. Magn Reson Med *29*, 311-316.

Koenig, S. H., and Kellar, K. E. (1995). Theory of $1/T_1$ and $1/T_2$ NMRD profiles of solutions of magnetic nanoparticles. Magn Reson Med *34*, 227-33.

Koenig, S. H., and Schillinger, W. E. (1969). Nuclear magnetic relaxation dispersion in protein solutions. I. Apotransferrin. J Biol Chem *244*, 3283-3289.

Korb, J.-P., and Bryant, R. G. (2002). Magnetic field dependence of proton spin-lattice relaxation times. Magn Reson Med *48*, 21-26.

Korb, J.-P., and Bryant, R. G. (2001). The physical basis for the magnetic filed dependence of spin-lattice relaxation rates in proteins and tissues. J Chem Phys *115*, 10964-10974.

Kwong, K. K., Belliveau, J. W., Chesler, D. A., Goldberg, I. E., Weisskoff, R. M., Poncelet, B. P., Kennedy, D. N., Hoppel, B. E., Cohen, M. S., Turner, R., Cheng, H.-M., Brady, T. J., and Rosen, B. R. (1992). Dynamic magnetic resonance imaging of human brain activity during primary sensory stimulation. Proc. Natl. Acad. Sci. USA *89*, 5675-5679.

Lahajnar, G., Benko, B., Rutar, V., and Zupancic, I. (1976). Proton magnetic relaxation dispersion in human fluoromethaemoglobin solutions. Int J Pept Protein Res *8*, 317-322.

Le Bihan, D., and Turner, R. (1992). The capillary network: a link between IVIM and classical perfusion. Magn Reson Med *27*, 171-8.

Lee, S. P., Silva, A. C., Ugurbil, K., and Kim, S. G. (1999). Diffusion-weighted spin-echo fMRI at 9.4 T: microvascular/tissue contribution to BOLD signal changes. Magn Reson Med *42*, 919-928.

Leenders, K. L., Perani, D., Lammertsma, A. A., Heather, J. D., Buckingham, P., Healy, M. J. R., Gibbs, J. M., Wise, R. J. S., Hatazawa, J., Herold, S., Beaney, R. P., Brooks, D. J., Spinks, T., Rhodes, C., Frackowiak, R. S. J., and Jones, T. (1990). Cerebral blood flow, blood volume and oxygen utilization: normal values and effect of age. Brain *113*, 27-47.

Li, D., Wang, Y., and Waight, D. J. (1998). Blood oxygen saturation assessment in vivo using T_2^* estimation. Magn Reson Med *39*, 685-690.

Li, J. G., Stanisz, G. J., and Henkelman, R. M. (1998). Integrated analysis of diffusion and relaxation of water in blood. Magn Reson Med *40*, 79-88.

Lindstrom, T. R., Koenig, S. H., Boussios, T., and Bertles, J. F. (1976). Intermolecular interactions of oxygenated sickle hemoglobin molecules in cells and cell-free solutions. Biophys J *16*, 679-689.

Look, D. C., and Locker, D. R. (1970). Time saving in measurement of NMR and EPR relaxation times. Rev Sci Instrum *41*, 250-251.

Lu, H., Golay, X., and van Zijl, P. C. M. (2002). Inter-voxel heterogeneity of event-related

fMRI responses as a function of T_1-weighting. Neuroimage *in press*.

Mäkelä, H. I., Gröhn, O. H., Kettunen, M. I., and Kauppinen, R. A. (2001). Proton exchange as a relaxation mechanism for T_1 in the rotating frame in native and immobilized protein solutions. Biochem Biophys Res Commun *289*, 813-818.

Marchal, G., Rioux, P., Petit-Taboue, M.-C., Sette, C., Travere, J.-M., La Poec, C., Courthenoux, P., Derlon, J.-M., and Baron, J.-C. (1992). Regional cerebral oxygen consumption, blood flow, and blood volume in healthy human aging. Arch Neurol *49*, 1013-1020.

Mathai, J. C., Mori, S., Smith, B. L., Preston, G. M., Mohandas, N., Collins, M., van Zijl, P. C., Zeidel, M. L., and Agre, P. (1996). Functional analysis of aquaporin-1 deficient red cells. The Colton-null phenotype. J Biol Chem *271*, 1309-1313.

Matwiyoff, N. A., Gasparovic, C., Mazurchuk, R., and Matwiyoff, G. (1990). The line shapes of the water proton resonances of red blood cells containing carbonyl hemoglobin, deoxyhemoglobin, and methemoglobin: implications for the interpretation of proton MRI at fields of 1.5T and below. Magn Reson Imag *8*, 295-301.

Matwiyoff, N. A., Gasparovic, C., Mazurchuk, R., and Matwiyoff, G. (1991). On the origin of paramagnetic inhomogeneity effects in whole blood. Magn Reson Med *20*, 144-50.

Menon, R. S., and Allen, P. S. (1990). Solvent proton relaxation of aqueous solutions of the serum proteins α_2-macroglobulin, fibrinogen, and albumin. Biophys J *57*, 389-396.

Meyer, M.-E., Yu, O., Eclancher, B., Grucker, D., and Chambron, J. (1995). NMR relaxation rates and blood oxygenation level. MRM *34*, 234-241.

Millet, O., Loria, J. P., Kroenke, C. D., Pons, M., and Palmer, A. G. I. (2000). The static magnetic field dependence of chemical exchange line broadening defined the NMR chemical shift time scale. J. Am. Chem. Soc. *122*, 2867-2877.

Moonen, C. T. W., and Bandettini, P. A. (1999). Functional MRI (Berlin: Springer-Verlag).

Morariu, V. V., Pop, V. I., Popescu, O., and Benga, G. (1981). Effects of temperature and pH on the water exchange through erythrocyte membranes: nuclear magnetic resonance studies. J Membr Biol *62*, 1-5.

Moseley, M. E., Cohen, Y., Mintorovitch, J., Chileuitt, L., Shimizu, H., Kucharczyk, J., Wendland, M. F., and Weinstein, P. R. (1990). Early detection of regional cerebral ischemia in cats: comparison of diffusion- and T_2-weighted MRI and spectroscopy. Magn Reson Med *14*, 330-346.

Nummi, P., Alanen, A., Nanto, V., and Kormano, M. (1986). Effect of hemolysis and clotting on proton relaxation times of blood. Acta Radiol Diagn (Stockh) *27*, 225-230.

Nusser, W., and Kimmich, R. (1990). Protein backbone fluctuations and NMR field cycling relaxation spectroscopy. J Phys Chem *94*, 5637-5639.

Ogawa, S., and Lee, T. M. (1990). Magnetic resonance imaging of blood vessels at high fields: in vivo and in vitro measurements and image simulation. Magn Reson Med *16*, 9-18.

Ogawa, S., Menon, R. S., Tank, D. W., Kim, S.-G., Merkle, H., Ellerman, J. M., and Ugurbil, K. (1993). Functional brain mapping by blood oxygenation level-dependent contrast magnetic resonance imaging: a comparison of signal characteristics with a biophysical model. Biophys. J. *64*, 803-812.

Ogawa, S., Tank, D. W., Menon, R., Ellermann, J. M., Kim, S. G., Merkle, H., and Ugurbil, K. (1992). Intrinsic signal changes accompanying sensory stimulation: functional brain mapping with magnetic resonance imaging. Proc Natl Acad Sci U S A *89*, 5951-5955.

Oja, J. M., Gillen, J. S., Kauppinen, R. A., Kraut, M., and van Zijl, P. C. (1999). Determination of oxygen extraction ratios by magnetic resonance imaging. J Cereb Blood Flow Metab *19*, 1289-1295.

Oja, J. M. E., Gillen, J., Kauppinen, R. A., Kraut, M., and van Zijl, P. C. M. (1999). Venous blood effects in spin echo fMRI of human brain. Magn. Reson. Med. *42*, 617-626.

Ordidge, R. J., Bendall, M. R., Gordon, R. E., and Conelly, A. (1985). Volume selection for in vivo spectroscopy. In Magnetic Resonance in Biology and Medicine, G. Gorvind, C. L. Khatrapal and A. Saran, eds. (New Delhi: Tata-McGraw-Hill), pp. 387-397.

Pauling, L., and Coryell, C. (1936). The Magnetic Properties and Structure of Hemoglobin, Oxyhemoglobin and Carbonmonoxy hemoglobin. Proc Natl Acad Sci U S A *22*, 210-216.

Powers, W. J. (1991). Cerebral hemodynamics in ischemic cerebrovascular disease. Ann Neurol *29*, 231-240.

Roch, A., and Muller, N. (1999). Theory of proton relaxation induced by superparamagnetic particles. J Chem Phys *110*, 5403-5411.

Santyr, G. E., Henkelman, R. M., and Bronskill, M. J. (1988). Variation in measured transverse relaxation in tissue resulting from spin locking with the CPMG sequence. J Magn Reson *79*, 28-44.

Santyr, G. E., Kay, I., henkelman, R. M., and Bronskill, M. J. (1990). Diffusive exchange analysis of two-component T_2 relaxation of red-blood-cell suspensions containing gadolinium. J Magn Reson *90*, 500-513.

Sette, G., Baron, J. C., Mazoyer, B., Levasseur, M., Pappata, S., and Crouzel, C. (1989). Local brain haemodynamics and oxygen metabolism in cerebrovascular disease. Positron emission tomography. Brain *112*, 931-951.

Sharan, M., Jones, M. D. J., Koehler, R. C., Traystman, R. J., and Popel, A. S. (1989). A compartmental model for oxygen transport in brain microcirculation. Ann Biomed Engin *17*, 13-38.

Silva, A. C., and Kim, S. G. (1999). Pseudo-continuous arterial spin labeling technique for measuring CBF dynamics with high temporal resolution. Magn Reson Med *42*, 425-429.

Silvennoinen, M. J., Clingman, C. S., Golay, X., Kauppinen, R. A., and van Zijl, P. C. M. (2001). Oxygenation and Hematocrit Dependence of Blood T_2 Relaxation at 1.5 T. In ISMRM 9th Scientific Meeting and Exhibition (Glasgow, UK, pp. 280.

Silvennoinen, M. J., Hakumäki, J. M., van Zijl, P. C. M., and Kauppinen, R. A. (1999). Exchange effects in blood T_2 at 9.4 T. In ISMRM 7th Scientific Meeting and Exhibition (Philadelphia, PA, USA.

Song, A. W., Wong, E. C., Tan, S. G., and Hyde, J. S. (1996). Diffusion weighted fMRI at 1.5 T. Magn Reson Med *35*, 155-8.

Spees, W. M., Yablonskiy, D. A., Oswood, M. C., and Ackerman, J. J. (2001). Water proton MR properties of human blood at 1.5 Tesla: magnetic susceptibility, T_1, T_2, T_2* and non-Lorentzian signal behavior. Magn Reson Med *45*, 533-542.

Springer, C. S. J. (1994). Bulk magnetic susceptibility frequencty shifts in cell suspension. NMR Biomed *7*, 192-202.

Stanisz, G. J., Li, J. G., Wright, G. A., and Henkelman, R. M. (1998). Water dynamics in human blood via combined measurements of T_2 relaxation and diffusion in the presence of gadolinium. Magn Reson Med *39*, 223-233.

Sullivan, S. G., Stern, A., Rosenthal, J. S., Minkoff, L. A., and Winston, A. (1988). NMR water-proton spin-lattice relaxation time of human red blood cells and red blood cell suspensions. FEBS Lett *234*, 349-352.

Thompson, R. T., Knispel, R. R., and Pintar, M. M. (1973). A study of the proton exchange in tissue water by spin relaxation in the rotating frame. Chem Phys Lett *22*, 335-337.

Thulborn, K. R., Waterton, J. C., Matthews, P. M., and Radda, G. K. (1982). Oxygenation dependence of the transverse relaxation time of water protons in whole blood at high field. Biochim. Biophys. Acta *714*, 265-270.

Toga, A. W., and Mazziotta, J. C. (1996). Brain Mapping: The Methods (San Diego: Academic Press).

Ugurbil, K., Hu, X., Chen, W., Zhu, X. H., Kim, S. G., and Georgopoulos, A. (1999). Functional mapping in the human brain using high magnetic fields. Philos Trans R Soc Lond B Biol Sci *354*, 1195-1213.

van Zijl, P. C., Eleff, S. M., Ulatowski, J. A., Oja, J. M., Ulug, A. M., Traystman, R. J., and Kauppinen, R. A. (1998). Quantitative assessment of blood flow, blood volume and blood oxygenation effects in functional magnetic resonance imaging. Nat Med *4*, 159-167.

Venu, K., Denisov, V. P., and Halle, B. (1997). Water ^{1}H magnetic relaxation dispersion in protein solutions. A quantitative assessment of internal hydration, proton exchange, and cross-relaxation. J. Am. Chem. Soc. *119*, 3122-3134.

Wang, D., Kreutzer, U., Chung, Y., and Jue, T. (1997). Myoglobin and hemoglobin rotational diffusion in the cell. Biophys J *73*, 2764-2770.

Waters, J. R. (2002). **Lecture slides for course Human Physiology**. http://www.bio.psu.edu /Courses/Spr2002/Biol141-sect901/powerpoint/All_the_circulatory_slides/sld006.htm 02/18/2002

Weisskoff, R. M., and Kiihne, S. (1992). MRI susceptometry: image-based measurement of absolute susceptibility of MR contrast agents and human blood. Magn Reson Med *24*, 375-383.

Weisskoff, R. M., Zuo, C. S., Boxerman, J. L., and Rosen, B. R. (1994). Microscopic susceptibility variation and transverse relaxation: theory and experiment. Magn Reson Med *31*, 601-610.

Weissleder, R., Moore, A., Mahmood, U., Bhorade, R., Benveniste, H., Chiocca, E. A., and Basilion, J. P. (2000). In vivo magnetic resonance imaging of transgene expression. Nat Med *6*, 351-355.

Williams, D. S., Detre, J. A., Leigh, J. S., and Koretsky, A. P. (1992). Magnetic resonance imaging of perfusion using spin inversion of arterial water. Proc Natl Acad Sci U S A *89*, 212-216.

Wong, E. C., Buxton, R. B., and Frank, L. R. (1997). Implementation of quantitative perfusion imaging techniques for functional brain mapping using pulsed arterial spin labeling. NMR Biomed *10*, 237-249.

Wright, G. A., Hu, B. S., and Macovski, A. (1991). Estimating oxygen saturation of blood in vivo with MR imaging at 1.5T. J. Magn. Reson. Imag. *1*, 275-283.

Wüthrich, K. (1986). NMR of proteins and nucleic acids (New York: John Wiley & Sons, Inc.).

Yablonskiy, D. A., and Haacke, E. M. (1994). Theory of NMR signal behavior in magnetically inhomogeneous tissues: the static dephasing regime. Magn Reson Med *32*, 749-763.

Ye, F. Q., and Allen, P. S. (1995). Relaxation enhancement of the transverse magnetization of water protons in paramagnetic suspensions of red blood cells. Magn Reson Med *34*, 713-720.

Zhou, J., and van Zijl, P. C. (1999). Perfusion imaging using FAIR with a short predelay. Magn Reson Med *41*, 1099-1107.

Zhu, X. H., and Chen, W. (2001). Observed BOLD effects on cerebral metabolite resonances in human visual cortex during visual stimulation: a functional (1)H MRS study at 4 T. Magn Reson Med *46*, 841-847.

Zimmermann, J. R., and Brittin, W. E. (1957). Nuclear Magnetic Resonance Studies in Multiple Phase Systems: Lifetime of a Water Molecule in an Adsorbing Phase on Silica Gel. J Phys Chem *61*, 1328-1333.

Zipp, A., Kuntz, I. D., and James, T. L. (1977). Hemoglobin-water interactions in normal and sickle erythrocytes by proton magnetic resonance T_{1p} measurements. Arch Biochem Biophys *178*, 435-441.